

# Calnexin polyclonal antibody

Calnexin (CNX), an unglycosylated resident ER transmembrane protein, together with Calreticulin (CRT), plays a key role in glycoprotein folding and its control within the ER, by interacting with folding intermediates via their monoglucosylated glycans. Calnexin associates with newly synthesized monomeric glycoproteins and only recognizes glycoproteins when they are incompletely folded. Furthermore, Calnexin has been demonstrated to function as a molecular chaperone capable of interacting with polypeptide segments of folding glycoproteins.

This antibody is covered by our [Worry-Free Guarantee](#).

Citations: 385

[View Online »](#)

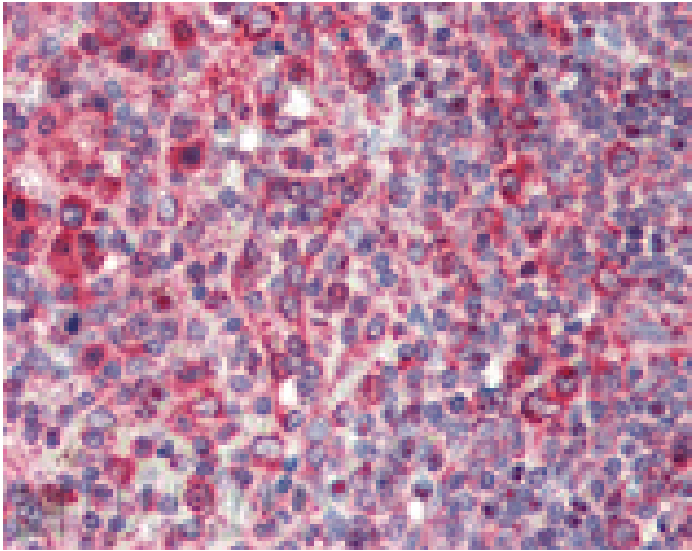
## Ordering Information

[Order Online »](#)

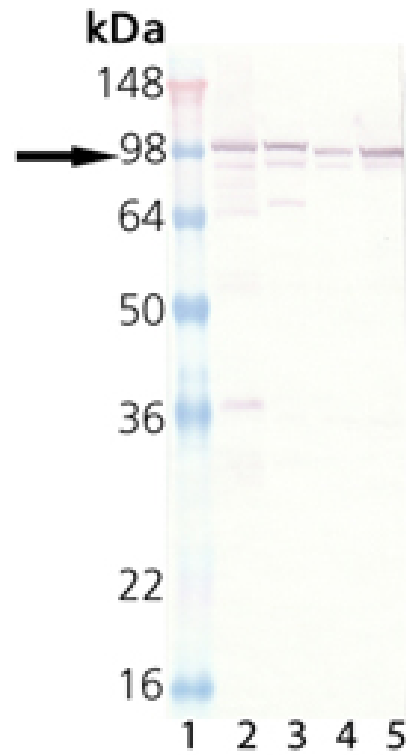
ADI-SPA-860-D	50µg
ADI-SPA-860-F	200µg

## Manuals, SDS & CofA

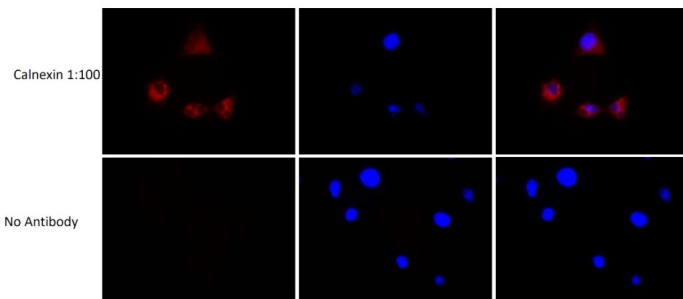
[View Online »](#)



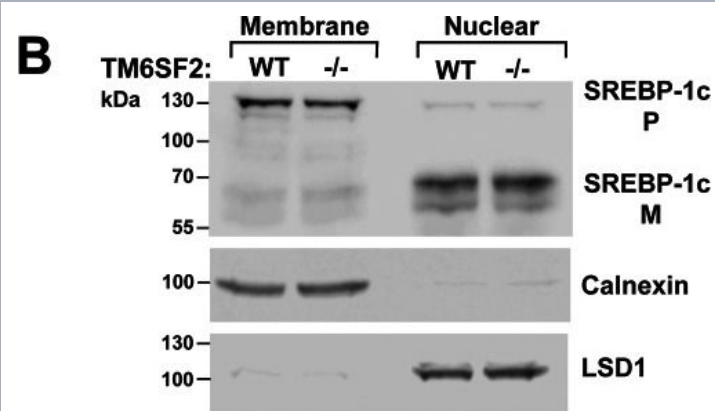
Immunohistochemistry analysis of human spleen tissue stained with Calnexin, pAb at 10µg/ml.



Western blot analysis: Lane 1: HeLa (heat shocked), Lane 2: Vero (heat shocked), Lane 3: Rat-2 (heat shocked), Lane 4: L-929 (heat shocked).

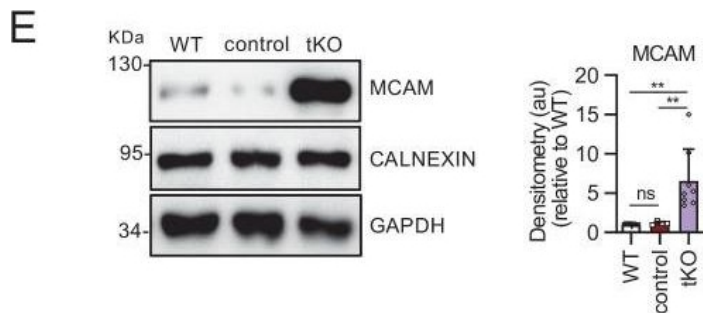


PANC-1 cells stained with anti-Calnexin pAb (ADI-SPA-860) using anti-rabbit 594 (Cell Signaling, 1:100 dilution) as secondary antibody.

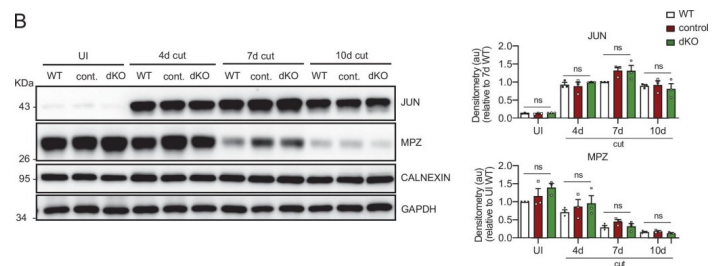


Relative mRNA levels of selected genes involved in cholesterol and triglyceride metabolism in the livers of WT and Tm6sf2<sup>-/-</sup> mice (A) and hepatic SREBP-1c cleavage (B). A, quantitative real-time PCR assays were performed to assess the relative levels of selected mRNAs in livers of the 13-week-old chow-fed male mice (5 mice/group) and in 11-week-old chow-fed female mice (6 mice/group) described in the legend to Fig. 3A. Expression levels were normalized to levels of 36B4 and expressed relative to levels of WT transcript. Values are means  $\pm$  S.E. (error bars). The official gene symbols were used for all of the genes with the following exceptions: ATGL (adipose TG lipase), PNPLA2; LXR $\alpha$ , NR1H3; PGC-1 $\alpha$ , PPARGC1A; L-PK, PKLR; PEPCCK, PCK1; ChREBP, MLXIPL. B, SREBP-1c regulation in Tm6sf2 KO mice. Nuclear and membrane fractions were isolated from livers of 18-week-old re-fed male mice (n = 4) by ultracentrifugation as described under "Experimental Procedures." Lysates from each mouse were pooled, and 40  $\mu$ g of pooled protein was size-separated on SDS-10% polyacrylamide gels. Proteins were transferred to nitrocellulose membranes and blotted with rabbit anti-mouse mSREBP-1c antibody. The bands were visualized by ECL and quantified using a LI-COR Odyssey Fc imager. The membranes were then stripped and reblotted with antibodies against calnexin and LSD1. The experiment was repeated with 13-week-old females, and the results were similar. \*, p < 0.05; \*\*\*\*, p < 0.0001.

Image collected and cropped by CiteAb under a CC-BY license from the following publication: Inactivation of Tm6sf2, a Gene Defective in Fatty Liver Disease, Impairs Lipidation but Not Secretion of Very Low Density Lipoproteins. *J Biol Chem* (2016)

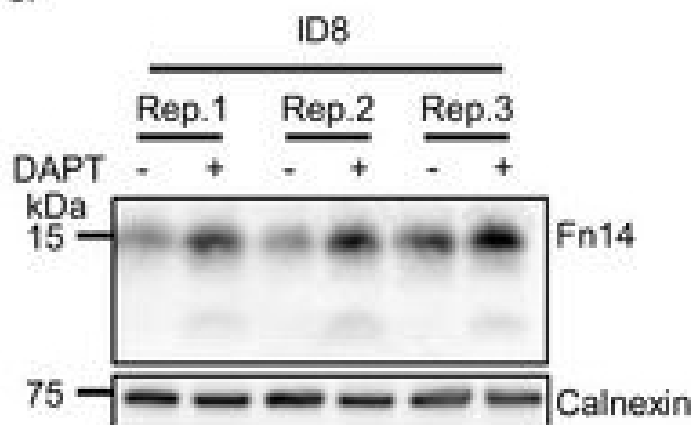


Melanocyte lineage markers are expressed by nonmyelinating Schwann cells of the Remak bundles in the sciatic nerves of the tKO. (A) mRNA for *Tyrp1* is dramatically increased by 1.081-fold in the tKO ( $3.35 \pm 0.71 \times 10^{-4}$  au in the tKO versus  $0.11 \pm 0.05 \times 10^{-6}$  au in controls;  $p = 0.0092$ ) whereas no changes were found in the cKO4, cKO7 neither dKO sciatic nerves. (B) mRNA for *Mcam* is also upregulated (5.13-fold) in the tKO ( $7.39 \pm 0.79 \times 10^{-4}$  au in the tKO versus  $1.44 \pm 0.06 \times 10^{-4}$  au in controls) with only minor or no changes at all for the other genotypes. The same although less marked (1.74-fold) for *Mitf* ( $0.87 \pm 0.09 \times 10^{-5}$  au in the tKO versus  $0.50 \pm 0.02 \times 10^{-5}$  au in controls;  $p = 0.0128$ ) (C) and *Ednrb* (4.1-fold;  $4.23 \pm 0.52 \times 10^{-5}$  au in the tKO versus  $1.04 \pm 0.09 \times 10^{-5}$  au in controls;  $p = 0.0032$ ) (D). RT-qPCR with mouse-specific primers for the indicated genes was performed. Graph shows a scatter plot for the  $\Delta C_t$  (which include also the mean  $\pm$  standard error [SE]) of the gene normalized to the housekeeping 18S. Four to five mice per genotype were used. Data were analyzed with the unpaired t-test with Welch's correlation. (E) MCAM protein levels in the sciatic nerves of the tKO. A representative Western blot of protein extracts from wild-type (C57BL/6), control and tKO sciatic nerves is shown. MCAM protein was increased by 7.6-fold in the tKO ( $9.93 \pm 1.75$  au in the tKO versus  $1.30 \pm 0.13$  in controls;  $p = 0.0003$ ). (F) NGFR protein was increased by 2.15-fold ( $2.16 \pm 0.29$  in the tKO versus  $1.005 \pm 0.09$  in controls;  $p = 0.0003$ ). Four to eight WB of the same number of animals per genotype were quantified. Data were analyzed with the one-way analysis of variance (ANOVA) Tukey's test. (G) MCAM signal colocalizes with SOX10. (H) MCAM signal colocalizes with NGFR. (I) MCAM is not expressed by myelin-forming Schwann cells (MPZ+). (J) Same happens with NGFR. (K) MCAM signal colocalizes with L1cam, a marker of the nonmyelin-forming Schwann cells of the Remak bundles. P60 sciatic nerves were fixed and submitted to immunofluorescence with the indicated antibodies. Nuclei were counterstained with Hoechst. Representative confocal images of sections obtained from the sciatic nerves of wild-type (WT), control, and tKO mice are shown. Scale bar: 20  $\mu$ m (\* $p < 0.05$ ; \*\* $p < 0.01$ ).

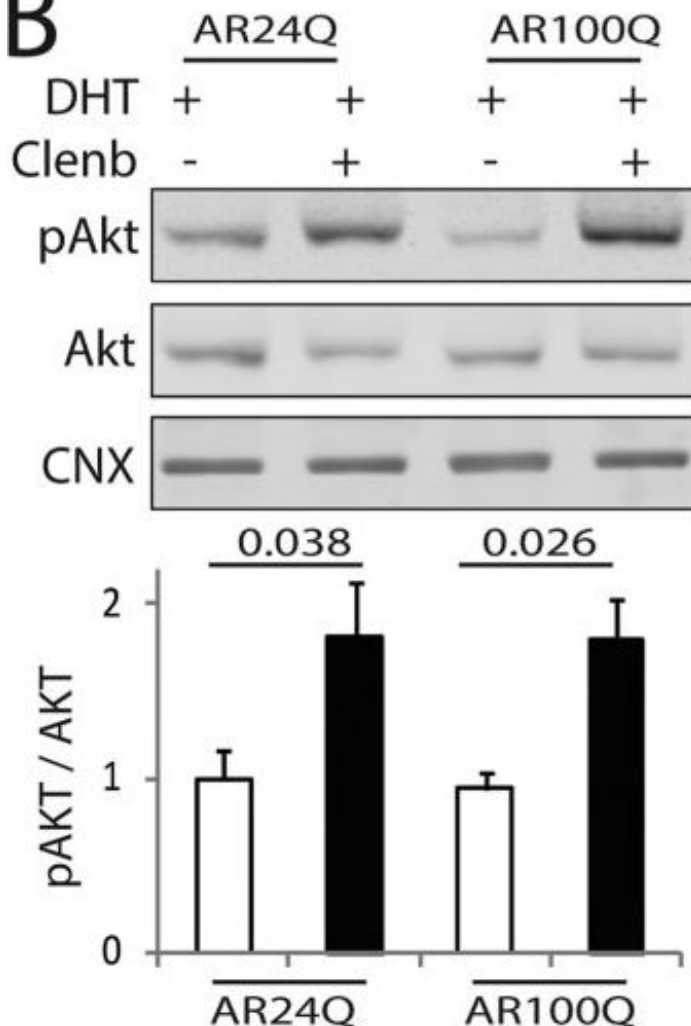


Myelin clearance and repair phenotype activation in the dKO mice. (A) A representative toluidine blue staining image of 4 days cut sciatic nerve of dKO and control mice is shown. The quantification of intact myelin sheaths showed no changes. Scale bar: 10  $\mu$ m. Four to five animals were used for the experiment. Data were analyzed with the unpaired t-test. (B) WB against JUN and MPZ supports that myelin clearance is normal in the dKO nerves. CALNEXIN and GAPDH were used as housekeeping. Three mice per genotype were analyzed independently by densitometry. To decrease the variability of standardizing for a condition with low expression, normalization was done for conditions with higher protein expression. Data were analyzed with the one-way analysis of variance (ANOVA) Tukey's test. (C) Repair phenotype activation was determined by measuring the expression of marker genes and comparing with the uninjured control nerve. As is shown only a slight increase in the expression of Jun at 1 day after cut in the dKO was found ( $3.71 \pm 0.24$  in the dKO versus  $2.35 \pm 0.22$  in the control;  $p = 0.0102$ ). RT-qPCR with mouse-specific primers for the indicated genes was performed and normalized to 18S rRNA. Graph shows the percentage of mRNA for each gene in the injured nerve normalized to the uninjured controls. A scatter plot is shown with the results obtained, which include also the mean  $\pm$  standard error (SE). Three to four mice per genotype were used. Data were analyzed with the unpaired t-test. Primer sequences and antibodies are listed online (Key Resources Table) (\* $p < 0.05$ ; \*\* $p < 0.01$ ; \*\*\* $p < 0.001$ ; ns: not significant). See source data file one online (graphs source data) for more details.

Image collected and cropped by CiteAb under a CC-BY license from the following publication: A genetic compensatory mechanism regulated by Jun and Mef2d modulates the expression of distinct class IIa Hdacs to ensure peripheral nerve myelination and repair. *Elife* (2022)

**G**

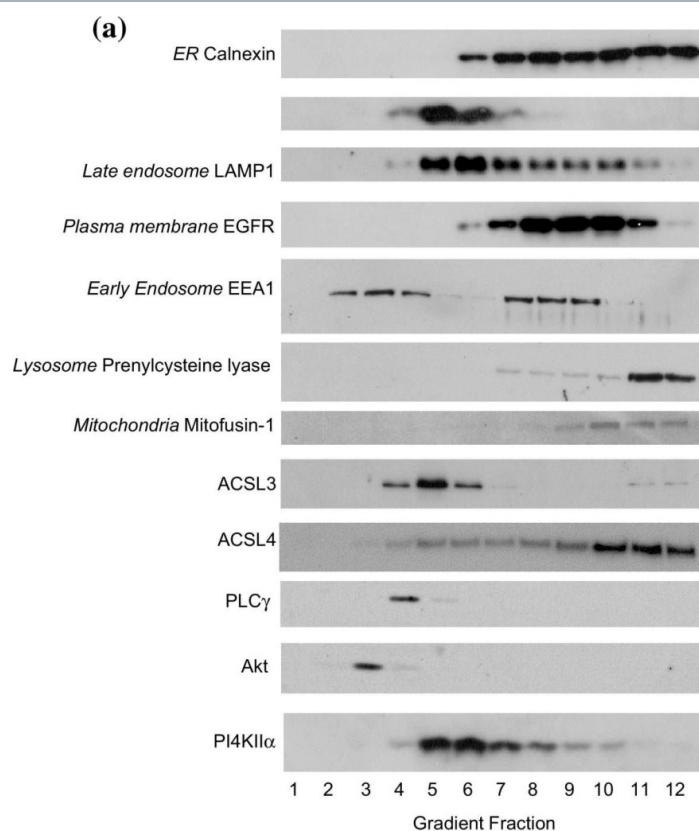
Endogenous Fn14 processing in mouse cell lines by  $\gamma$ -secretase. Mouse glioblastoma cell line GL261 showed cellular accumulation of Fn14 upon  $\gamma$ -secretase inhibition. Cells were treated overnight with  $\gamma$ -secretase inhibitor DAPT (1  $\mu$ M) or vehicle. Lysates of biological replicates (Rep.) were blotted for Fn14 with an antibody that targets the C-terminal end of the protein, or against calnexin as loading control. B. Quantification of blot in panel (A). Intensity values of Fn14 were normalized to the respective Calnexin loading control. The average of the control condition, where the cells were only treated with vehicle (DMSO), was consecutively normalized to 1. C. Conditioned media of the GL261 cells from panel (A) were collected, and sFn14 levels were measured by ELISA. D. Mouse breast cancer cell line 4T1 showed cellular accumulation of Fn14 upon  $\gamma$ -secretase inhibition. Cells were treated overnight with  $\gamma$ -secretase inhibitor DAPT (1  $\mu$ M) or vehicle. Lysates were blotted for Fn14 with an antibody that targets the C-terminal end of the protein, or against calnexin as loading control. E. Quantification of blot in panel (D). Intensity values of Fn14 were normalized to the respective calnexin loading control. The average of the control condition, where the cells were only treated with vehicle (DMSO), was consecutively normalized to 1. F. Conditioned media of the 4T1 cells from panel (D) were collected and sFn14 levels measured by ELISA. G. Mouse ovarian cancer cell line ID8 showed cellular accumulation of Fn14 upon  $\gamma$ -secretase inhibition. Cells were treated overnight with  $\gamma$ -secretase inhibitor DAPT (1  $\mu$ M) or vehicle. Lysates were blotted for Fn14 with an antibody that targets the C-terminal end of the protein, or against calnexin as loading control. H. Quantification of blot in panel (G). Intensity values of Fn14 were normalized to the respective calnexin loading control. The average of the control condition, where the cells were only treated with vehicle (DMSO), was consecutively normalized to 1. I. Conditioned media of the ID8 cells from panel (G) were collected and sFn14 levels measured by ELISA. J,

**B**

Clenbuterol mitigates the atrophy induced by polyglutamine-expanded AR in C2C12 myotubes. (A) Upper panels, representative bright-field images of C2C12 myotubes expressing AR24Q and AR100Q treated with vehicle, DHT (10 nM), and clenbuterol (clenb, 10  $\mu$ M) for 14 DIV. Bottom panel, myotube width analysis. Graph, mean  $\pm$  SEM,  $n$  = 3 independent experiments. Two-way ANOVA + SNK. NS, non-significant. Bar, 25  $\mu$ m. (B,C) Western blotting analysis of phosphorylated and total Akt (B) and CREB (C) in C2C12 myotubes expressing AR24Q and AR100Q and cultured as in (A). Phosphorylated and total Akt and CREB were detected with specific antibodies, and calnexin (CNX) was used as loading control. Graph, mean  $\pm$  SEM,  $n$  = 6 (B) and 5 (C) independent experiments. Two-way ANOVA + SNK.

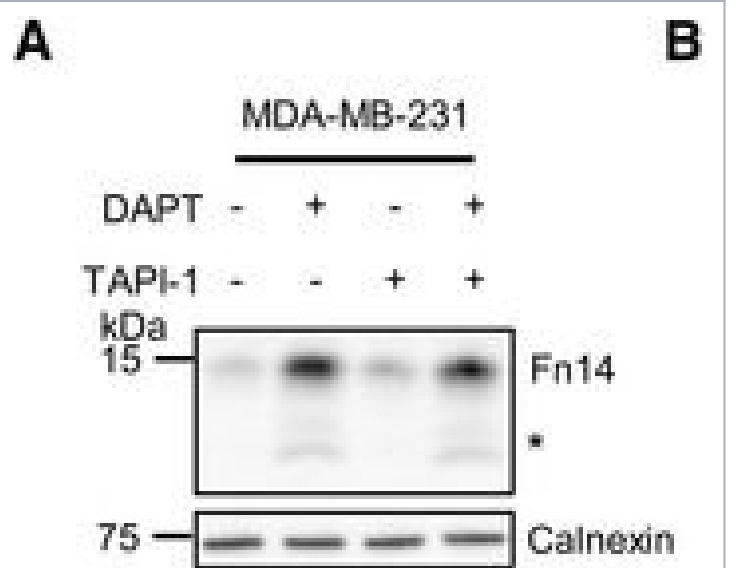
Image collected and cropped by CiteAb under a CC-BY license from the following publication: Beta-agonist stimulation ameliorates the phenotype of spinal and bulbar muscular atrophy mice and patient-derived myotubes. *Sci Rep* (2017)



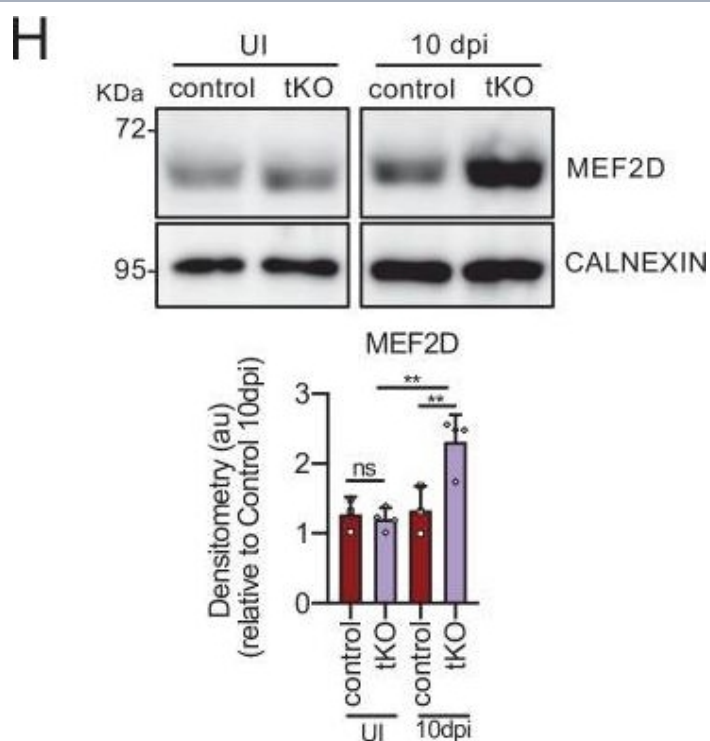


Equilibrium distributions of organelle marker proteins, ACSL3 and ACSL4 in HT1080 sucrose density gradient fractions. a Equal volumes of all HT1080 subcellular fractions were subjected to SDS-PAGE separation and immunoblotted for the ER marker protein calnexin; the TGN-endosomal protein syntaxin-6; the late endosomal protein LAMP1; the plasma membrane-associated EGFR, the early endosome-recruited protein EEA1; the lysosomal protein prenylcysteine lyase and the mitochondrial protein mitofusin-1, ACSL3 and ACSL4, and the inositol phospholipid-dependent enzymes Akt, PLC $\gamma$  and PI4KII $\alpha$ . Data presented are representative of experiments repeated 3–4 times with similar results. b The relative normalised distributions of anti-ACSL3 and anti-ACSL4 immunoreactivities in the gradient fractions. Western blotting signals were quantified using imageJ software. Data are representative of experiments repeated 3–4 times with similar results

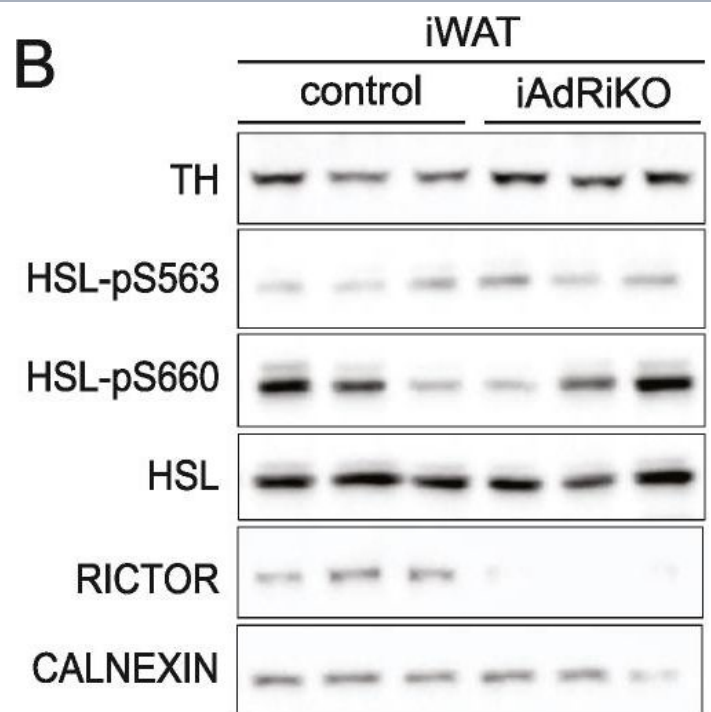
Image collected and cropped by CiteAb under a CC-BY license from the following publication: The endogenous subcellular localisations of the long chain fatty acid-activating enzymes ACSL3 and ACSL4 in sarcoma and breast cancer cells. *Mol Cell Biochem* (2018)



Endogenous Fn14 is processed by protease  $\gamma$ -secretase. Human breast cancer cell line MDA-MB-231 shows cellular accumulation of Fn14 upon  $\gamma$ -secretase inhibition. The cells were treated overnight with  $\gamma$ -secretase inhibitor DAPT (1  $\mu$ M), broad-spectrum metalloprotease inhibitor TAPI-1 (50  $\mu$ M), or the corresponding amount of vehicle DMSO as indicated. Lysates were blotted for Fn14 with an antibody that targets the C-terminal end of the protein, or against calnexin as loading control. The asterisk labels an N-terminally truncated form of Fn14. Quantification of blots from panel (A). The control condition, where the cells were only treated with vehicle (DMSO), was used as baseline, and its average normalized to 1. Human ovarian cancer cell line SKOV-3 shows cellular accumulation of Fn14 upon  $\gamma$ -secretase inhibition. The cells were treated overnight with  $\gamma$ -secretase inhibitor DAPT (1  $\mu$ M), broad-spectrum metalloprotease inhibitor TAPI-1 (50  $\mu$ M), or corresponding amount of vehicle DMSO as indicated. Lysates were blotted for Fn14 with an antibody that targets the C-terminal end of the protein, or against calnexin as loading control. The asterisk labels an N-terminally truncated form of Fn14. Quantification of blot from panel (C). The control condition, where the cells were only treated with vehicle (DMSO), was used as baseline, and its average normalized to 1. sFn14 is reduced upon  $\gamma$ -secretase inhibition in MDA-MB-231 cells. Conditioned media of the treated cells were collected after overnight DAPT (1  $\mu$ M) or vehicle treatment. sFn14 concentration was measured by human Fn14 ELISA. sFn14 is reduced upon  $\gamma$ -secretase inhibition in SKOV-3 cells. Conditioned media of the treated cells were collected after 48 h DAPT (1  $\mu$ M) or vehicle treatment. sFn14 concentration was measured by human Fn14 ELISA. Data Information: All quantification data are shown as mean  $\pm$  SEM. All the panels have N = 3 biological replicates. For panels (B) and (D), the tested conditions were compared

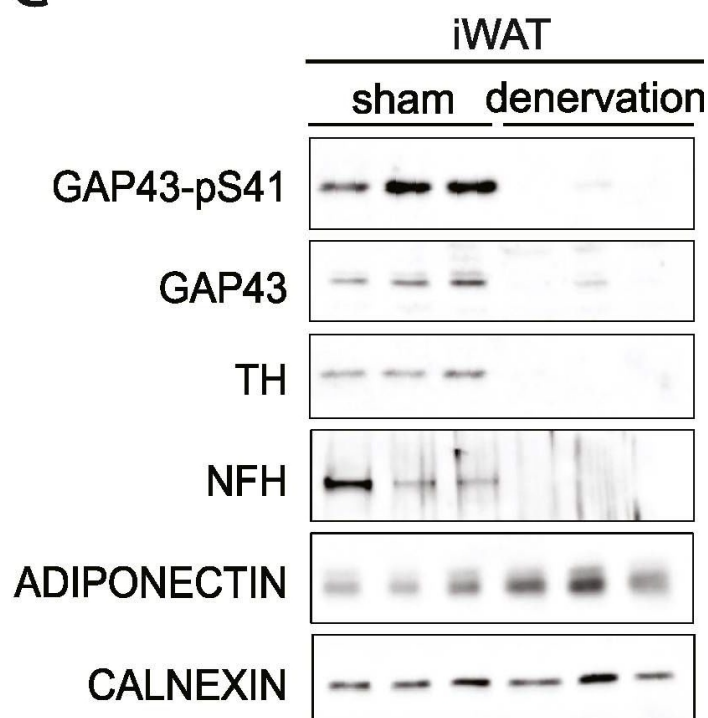


MEF2D mediates Hdac9 de novo expression in the tKO. (A) Hdac9 expression is notably induced in the sciatic nerves of the adult (P60) tKO mice ( $6.48 \pm 0.53 \times 10^{-6}$  au the tKO versus  $1.46 \pm 0.28 \times 10^{-6}$  in the control;  $p < 0.0001$ ). Only minor changes were observed in the cKO4 and cKO7. Four to eight mice per genotype were used. Unpaired t-test was used for comparisons. (B) Hdac9 expression is increased from early postnatal development of the tKO nerve. At P2 we found  $1.67 \pm 0.13 \times 10^{-6}$  au in the tKO versus  $0.39 \pm 0.03 \times 10^{-6}$  in the controls ( $p < 0.0001$ ) and at P8 we found  $3.43 \pm 0.52 \times 10^{-6}$  au in the tKO versus  $0.65 \pm 0.09 \times 10^{-6}$  in the controls ( $p < 0.0001$ ). RT-qPCR with mouse-specific primers for Hdac9 was performed. The scatter plot, which include also the mean  $\pm$  standard error (SE), shows the expression of Hdac9 normalized to the housekeeping 18S. Four to five mice per genotype were used. Data were analyzed with the unpaired t-test with Welch's correlation. (C) ChIP-qPCR with anti-H3K9Ac of adult (P60) sciatic nerves of tKO and control mice. Three different experiments of four to five animals per genotype are shown. Data were normalized to the IgG value as shown as relative enrichment. Unpaired t-test was used for comparisons. (D) Alignment of the reads of the RNA-seq from three individual sciatic nerves of control and three tKO mice, both uninjured and at 20 days post crush (20 dpi). Hdac9 gene is transcribed at detectable levels in the sciatic nerve of the uninjured tKO mice, whereas it is almost nondetectable in the control sciatic nerves. The tKO mice (but not the controls) increase additionally the expression of Hdac9 gene during remyelination (20 dpi). (E) mRNA levels of Hdac9 (as FPKMs) at 0, 1, 10, and 20 days post crush (dpi) in the RNA-seq experiment. Two-way analysis of



Sensory but not sympathetic innervation is altered upon loss of adipose mTORC2. (A) 2D representatives of a 3D reconstruction of inguinal WAT (iWAT) four weeks after tamoxifen treatment immunostained with tyrosine hydroxylase (TH; yellow). (A1-2) Low magnification projection of sympathetic neuronal network in control and iAdRiKO mice (N = 4; 5). Scale bar = 500  $\mu$ m. (A3-4) High magnification projection of sympathetic neurons in iWAT parenchyma of control mice and iAdRiKO (N = 19; 10). Scale bar = 100  $\mu$ m. (B) Immunoblot analysis of iWAT from control and iAdRiKO mice four weeks after tamoxifen treatment. Hormone-sensitive lipase (HSL). (n = 6; 6). (C) 2D representatives of a 3D reconstruction of iWAT four weeks after tamoxifen treatment immunostained with calcitonin gene-related peptide (CGRP; magenta). (C1-2) Low magnification projection of sensory neuronal network in control and iAdRiKO mice (N = 12; 19). Scale bar = 500  $\mu$ m. (C3-4) Low magnification cross section of sensory neuronal network in control and iAdRiKO mice (N = 12; 19). Nerve bundle (1), innervation along blood vessel (2), tissue autofluorescence (green). Scale bar = 500  $\mu$ m. (C5-6) High magnification projection of sensory neurons in iWAT parenchyma of control mice and iAdRiKO (N = 16; 11). Scale bar = 100  $\mu$ m. (C7-8) High magnification cross section of neurons in control and iAdRiKO mice (N = 16; 11). Innervation along blood vessel (2), parenchymal innervation (3), tissue autofluorescence (green). Scale bar = 100  $\mu$ m. (D) Quantification of the total neurite length of CGRP-positive neurons in iWAT parenchyma of control mice and iAdRiKO four weeks after tamoxifen treatment (N = 6).

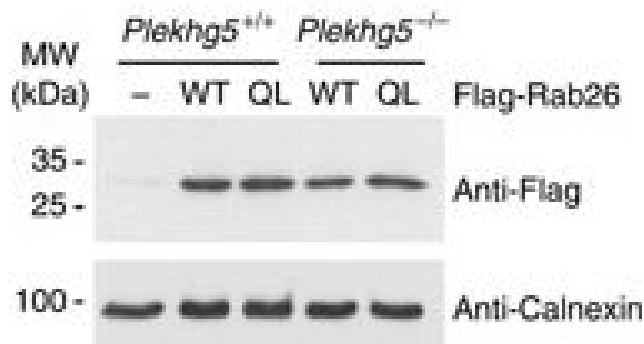
C



GAP43 expression is downregulated in CGRP-positive neurons upon loss of adipose mTORC2. (A) Immunoblot analysis of inguinal WAT (iWAT) tissue from control and iAdRiKO mice two weeks after tamoxifen treatment. (n = 6; 6). (B) Immunoblot analysis of iWAT tissue from control and iAdRiKO mice four weeks after tamoxifen treatment. (n = 6; 6). (C) Immunoblot analysis of surgically denervated iWAT depot (denervation) compared to iWAT depot from sham-operated mice (sham). Neurofilament heavy polypeptide (NFH). (n = 5; 5). (D) Representative image of a large nerve bundle in iWAT of control mice immunostained with growth-associated protein 43 (GAP43)-pS41 and calcitonin gene-related peptide (CGRP). (N = 11; 9). (E) Representative image of a large nerve bundle in iWAT of control mice immunostained with GAP43-pS41 and tyrosine hydroxylase (TH). (N = 19; 11).

Image collected and cropped by CiteAb under a CC-BY license from the following publication: Adipose mTORC2 is essential for sensory innervation in white adipose tissue and whole-body energy homeostasis. *Mol Metab* (2022)

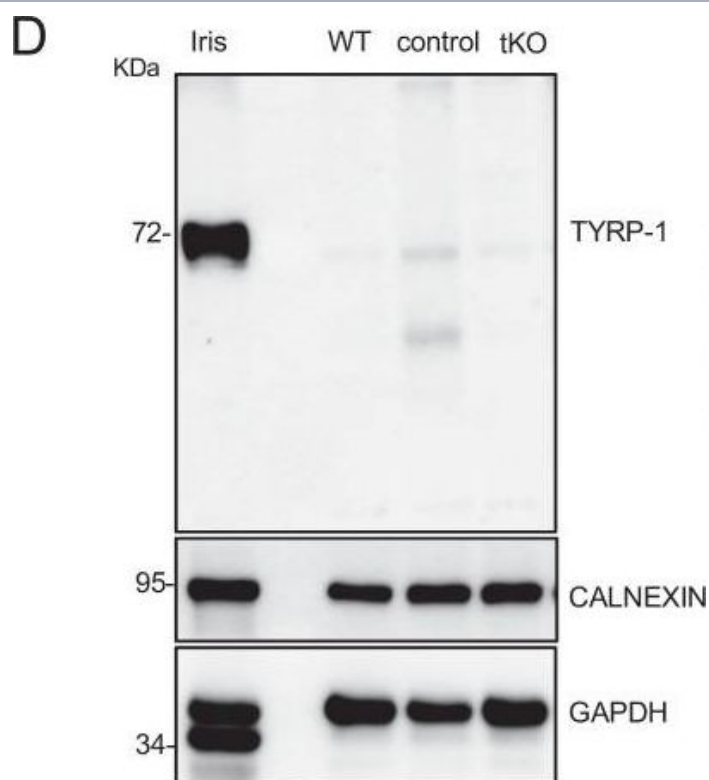
9



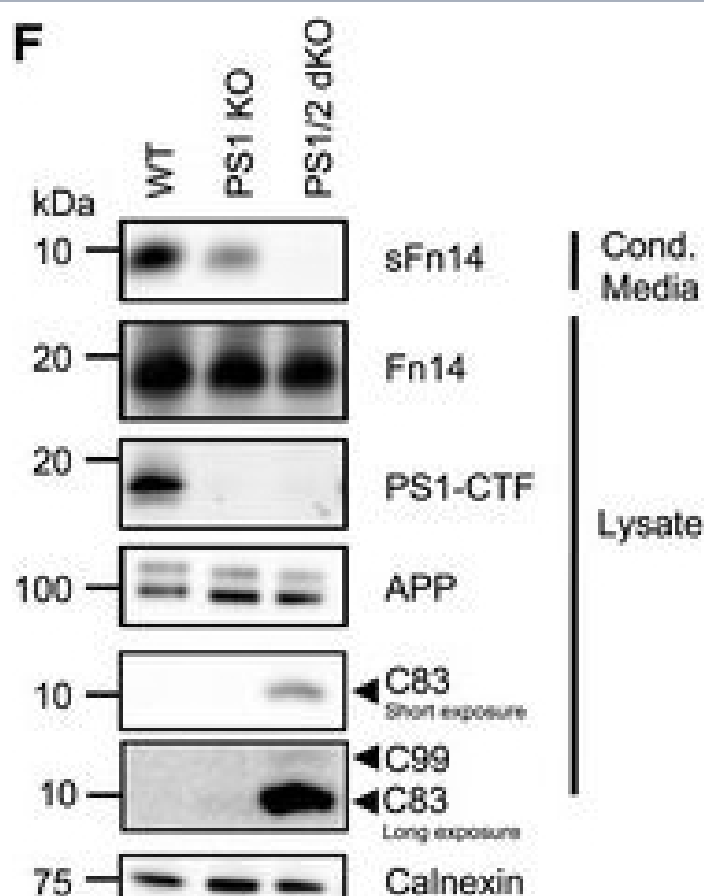
Expression of constitutively active Rab26 rescues axonal growth and autophagy defects in Plekhhg5-deficient cells. a Representative images of GFP-Rab26-WT or GFP-Rab26-QL positive structures in axons of control cells and Plekhhg5-deficient cells. Scale bar: 10  $\mu$ m. b Morphology of GFP, GFP-Rab26-WT or GFP-Rab26-QL expressing motoneurons cultured for 7 days. Scale bar: 100  $\mu$ m. c, d Size and number of axonal EGFP-Rab26 structures. e Axon length of GFP, GFP-Rab26-WT, or GFP-Rab26-QL expressing motoneurons isolated from Plekhhg5+/+ and Plekhhg5-/- mice (each data point represents one individual experiment with 15 cells analyzed in each experiment; mean  $\pm$  SEM; two-way ANOVA). f Scheme of lentiviral vectors for simultaneous expression of RFP-GFP-LC3 and Flag-Rab26-WT or Flag-Rab26-QL, respectively. g Western blot analysis of Flag-Rab26-WT and Flag-Rab26-QL expression. Images have been cropped for presentation. Full size images are presented in Supplementary Fig. 7. h Motoneurons of Plekhhg5+/+ and Plekhhg5-/- mice expressing mRFP-GFP-LC3 and Flag-Rab26-WT or Flag-Rab26-QL were cultured for 7 days and the number of mRFP-GFP-LC3 positive structures was analyzed. Scale bar: 10  $\mu$ m. i Number of autophagosomes and autolysosomes upon expression of Flag-Rab26-WT and Flag-Rab26-QL (three independent experiments with 10 cells analyzed in each experiment; mean  $\pm$  SEM; two-way ANOVA; Bonferroni post-test)

Image collected and cropped by CiteAb under a CC-BY license from the following publication: Plekhhg5-regulated autophagy of synaptic vesicles reveals a pathogenic mechanism in motoneuron disease. *Nat Commun* (2017)

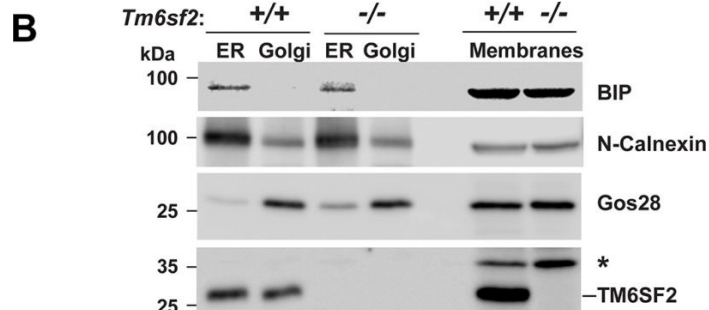




Characterizing the tKO mice. (A) Representative TEM images and morphometric analysis of the Remak bundles of single KO and dKO show no major changes in the segregation of the small size axons in these mice. 800–1000 axons from 3 to 4 animals per genotype were counted. Mixed model analysis of variance (ANOVA) with Bonferroni post hoc test was used for comparisons. Scale bar: 1  $\mu$ m. (B) Melanocyte lineage genes are upregulated during early development. P2, P8, and P21 mouse sciatic nerves were removed and total RNA extracted. RT-qPCR with mouse-specific primers for the indicated genes was performed and normalized to 18S rRNA. Graph shows the percentage of mRNA for each gene in the tKO normalized to the control littermates. A scatter plot is shown with the results obtained, which include also the mean  $\pm$  standard error (SE). 4/5 mice per genotype and age were used. Data were analyzed with the unpaired t-test. (C) A representative Western blot of protein extracts obtained from the sciatic nerves of P8 WT, control, and tKO mice is shown. CALNEXIN was used as a protein loading control. Densitometric analysis was done for 4 WB and normalized the WT. Data were analyzed with the one-way ANOVA Tukey's test. (D) The mRNA for *Tyrp1* is not translated to protein. A representative Western blot of protein extracts obtained from the sciatic nerves of adult WT, control, and tKO mice is shown. Iris was used as a positive control. CALNEXIN and GAPDH were used as protein loading controls. Because GAPDH is a doublet in iris, normalization was performed exclusively to CALNEXIN. Primer sequences and antibodies are listed online (Key Resources Table) (\* $p < 0.05$ ; \*\* $p < 0.01$ ; \*\*\* $p < 0.001$ ; ns: no significant). See

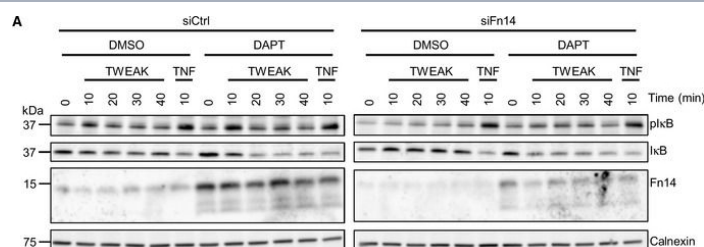


Fn14 is processed by the protease  $\gamma$ -secretase. Domain structure of Fn14. Fn14 has a short, compact N-terminal extracellular domain. It consists of 53 amino acids that contain three disulfide bridges (dashed lines) that form the cysteine-rich domain, CRD (red). Fn14 has a single transmembrane domain (blue) and a short C-terminal cytosolic tail with a TRAF binding site (green) important for its signaling function. Protein N- and C-termini (N, C) are indicated. Detection of sFn14 in conditioned media. HEK293E cells were transfected with either empty vector or a plasmid encoding human Fn14 that bears an N-terminal HA-tag and a C-terminal double FLAG-tag. Conditioned media and lysates of the transfected cells were collected and analyzed by immunoblotting with the indicated antibodies. Calnexin served as a loading control. Shown are representative blots from N = 3 experiments. Generation of sFn14 is sensitive to the  $\gamma$ -secretase inhibitor DAPT. HEK293E cells were transfected with either Fn14 or C99 (C-terminal fragment of APP), both containing a N-terminal HA-tag and C-terminal double FLAG-tag. One day after transfection, cells were treated with  $\gamma$ -secretase inhibitor DAPT (1  $\mu$ M), broad-spectrum metalloprotease inhibitor TAPI-1 (50  $\mu$ M), or the corresponding amount of vehicle DMSO as indicated. The conditioned media and the lysates were blotted with anti-HA antibody. Shown are representative blots from N = 4 experiments. Schematic representation of Fn14 shedding by the  $\gamma$ -secretase complex.  $\gamma$ -Secretase is a hetero-tetrameric complex consisting of the indicated subunits, with presenilin being the catalytic subunit. The structure of the  $\gamma$ -secretase complex is shown.



Subcellular localization of TM6SF2. A, primary hepatocytes from 8-week-old female mice on a chow diet were plated on collagen-coated coverslips for 4 h, fixed, and stained with antibodies against markers for the ER (calnexin (CANX)), cis-Golgi (receptor-binding cancer antigen expressed on SiSo cells (RCAS1)), and Golgi (Giantin (GOLGB1) (green, left column) and TM6SF2 (red, middle column)). The merged signal from both channels (yellow, right column) shows subcellular co-localization. All images were taken using a  $\times 63$  oil immersion objective. Scale bar, 10  $\mu$ m. B, immunoaffinity isolation of ER and Golgi complex from mouse liver. ER and Golgi fractions were prepared from mouse liver microsomes by immunoaffinity chromatography as described under "Experimental Procedures." Microsome membranes were dissolved in RIPA buffer, and equal volumes were separated on 10% SDS-PAGE and immunoblotting as described under "Experimental Procedures." BiP, binding immunoglobulin protein; Gos28, Golgi SNAP receptor complex member 1; \*, nonspecific band.

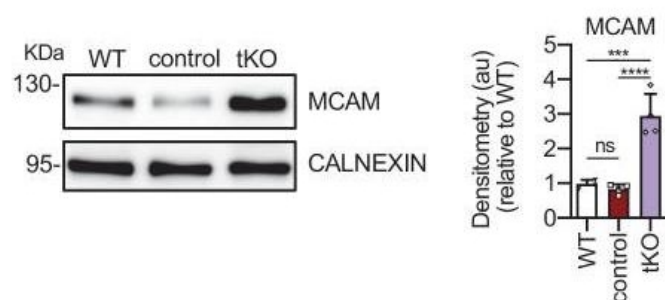
Image collected and cropped by CiteAb under a CC-BY license from the following publication: Inactivation of Tm6sf2, a Gene Defective in Fatty Liver Disease, Impairs Lipidation but Not Secretion of Very Low Density Lipoproteins. *J Biol Chem* (2016)



Inhibiting  $\gamma$ -secretase in MDA-MB-231 cells enhances Fn14 mediated NF $\kappa$ B signaling. MDA-MB-231 cells were transfected with an siRNA pool against human Fn14 or nontargeting control (Ctrl) siRNA. A day after transfection, cells were treated with  $\gamma$ -secretase inhibitor DAPT (1  $\mu$ M) or vehicle overnight. Either TWEAK (100 ng/ml) or positive control TNF (10 ng/ml) were applied for indicated time points. The cell lysate was blotted against pIkB and IkB to evaluate NF $\kappa$ B activation or against Fn14 to verify the effect of the DAPT and siFn14 treatment, or against calnexin as a loading control. Shown are representative blots from N = 4 experiments. MDA-MB-231 cells were treated with  $\gamma$ -secretase inhibitor DAPT (1  $\mu$ M) or vehicle overnight. TWEAK (100 ng/ml) was applied for 10 min. The cell lysate was blotted against pP65 and P65 to evaluate NF $\kappa$ B activation or against  $\beta$ -actin as a loading control. Shown are representative blots from N = 3 experiments. The dashed vertical line indicates that sample were run on the same blot but not directly next to each other.

Image collected and cropped by CiteAb under a CC-BY license from the following publication: Proteolytically generated soluble Tweak Receptor Fn14 is a blood biomarker for  $\gamma$ -secretase activity. *EMBO Mol Med* (2022)

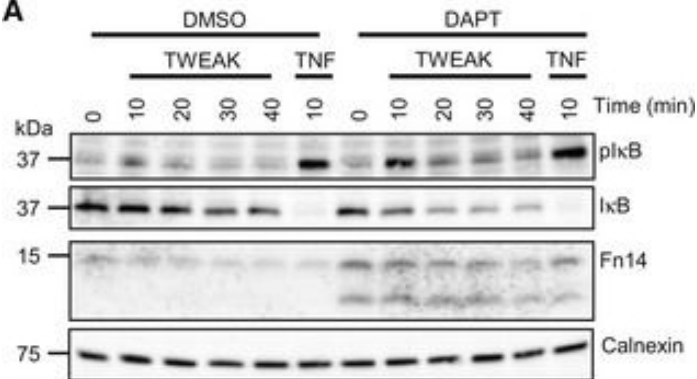
C



Characterizing the tKO mice. (A) Representative TEM images and morphometric analysis of the Remak bundles of single KO and dKO show no major changes in the segregation of the small size axons in these mice. 800–1000 axons from 3 to 4 animals per genotype were counted. Mixed model analysis of variance (ANOVA) with Bonferroni post hoc test was used for comparisons. Scale bar: 1  $\mu$ m. (B) Melanocyte lineage genes are upregulated during early development. P2, P8, and P21 mouse sciatic nerves were removed and total RNA extracted. RT-qPCR with mouse-specific primers for the indicated genes was performed and normalized to 18S rRNA. Graph shows the percentage of mRNA for each gene in the tKO normalized to the control littermates. A scatter plot is shown with the results obtained, which include also the mean  $\pm$  standard error (SE). 4/5 mice per genotype and age were used. Data were analyzed with the unpaired t-test. (C) A representative Western blot of protein extracts obtained from the sciatic nerves of P8 WT, control, and tKO mice is shown. CALNEXIN was used as a protein loading control. Densitometric analysis was done for 4 WB and normalized the WT. Data were analyzed with the one-way ANOVA Tukey's test. (D) The mRNA for *Tyrp1* is not translated to protein. A representative Western blot of protein extracts obtained from the sciatic nerves of adult WT, control, and tKO mice is shown. Iris was used as a positive control. CALNEXIN and GAPDH were used as protein loading controls. Because GAPDH is a doublet in iris, normalization was performed exclusively to CALNEXIN. Primer sequences and antibodies are listed online (Key Resources Table) (\*p < 0.05; \*\*p < 0.01; \*\*\*p < 0.001; ns: no significant). See source data file one online (graphs source data) for more details.

Image collected and cropped by CiteAb under a CC-BY license from the following publication: A genetic compensatory mechanism regulated by Jun and Mef2d modulates the expression of distinct class IIa Hdacs to ensure peripheral nerve myelination and repair. *Elife*

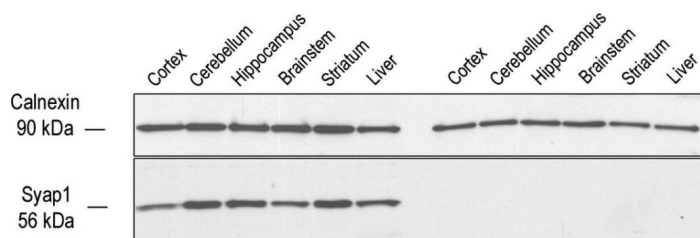
A



Inhibiting  $\gamma$ -secretase in glioblastoma cell line U87 enhances Fn14 mediated NFκB signaling. U87 cells were treated with  $\gamma$ -secretase inhibitor DAPT (1  $\mu$ M) or vehicle overnight. Either TWEAK (100 ng/ml) or positive control TNF (10 ng/ml) were applied for indicated time points. The cell lysate was blotted against pIκB and IκB to evaluate NFκB activation or against Fn14 to verify the effect of the DAPT and siFn14 treatment, or against calnexin as a loading control. Shown are representative blots from N = 4–5 experiments. U87 cells showed cellular accumulation of Fn14 upon  $\gamma$ -secretase inhibition. 0 min time point samples of Fn14 blot in panel (A) were quantified, normalized to the respective calnexin loading control and consecutively normalized to vehicle control average. Shown is the Fn14 intensity relative (rel.) to the DMSO control (N = 4).  $\gamma$ -Secretase inhibition by DAPT does not alter NFκB stimulation through TNF. U87 cells treated with TNF (10 ng/ml) for 10 min and the NFκB activation reported as ratio of pIκB to total IκB. Shown is the pIκB/IκB ratio relative (rel.) to the DMSO control (N = 5). D, E Quantification of the IκB (D) and pIκB (E) blots in panel (A). The measurements were normalized to the 0 min time point. N = 5 biological replicates. F The TWEAK stimulation of Fn14 and activation of NFκB is represented as ratio of pIκB to total IκB, taken from quantifications in (D) and (E). Shown is the pIκB/IκB ratio relative (rel.) to the 0 min time point. N = 5 biological replicates. Data information: All quantification data are shown as mean  $\pm$  SEM. The P-values that are above 0.05 have not been included into the panels. For panel (B) and (C), two-tailed unpaired t-tests were used. For panels (D) and (E), RM two-way ANOVAs with Šidák's multiple comparison test have been applied. For panel (F), two-tailed unpaired t-test have been applied for each time point. For all the panels, the number of biological replicates is reported in the corresponding panel legend.

Image collected and cropped by CiteAb under a CC-BY license from the following publication: Proteolytically generated soluble Tweak Receptor Fn14 is a blood biomarker for  $\gamma$ -secretase activity. *EMBO Mol Med* (2022)

b



Verification of Syap1 knockout and demonstration of Syap1 protein expression in different tissues. a qRT-PCR with mRNA from mouse cortex and primers connecting Syap1 exon-3 and exon-4 demonstrates that intact transcript levels are reduced in the Syap1<sup>tm1a</sup> mutant (curves 3, 4) by a factor of ~30 compared to wild type (curves 1, 2). Curve 5 indicates background (no reverse transcriptase). b Lysates of the indicated tissues analyzed by Western blots show comparable levels of Syap1 protein expression in all tested brain regions of wild-type mice. However, the protein is also detected in non-neural tissues such as liver (left half of blot). No Syap1 signals are obtained for tissues from Syap1<sup>tm1a</sup> mutant mice (right half of blot). c No trace of the Syap1 protein is detected by Western blots in lysates of hippocampus from Syap1<sup>tm1a</sup> mutant (lane 2) even after increased protein loading and extended exposure. The two weak upper bands are unspecific, and the weak lower bands presumably represent Syap1 degradation products. Top parts of blots in b and c: Calnexin signals as loading controls

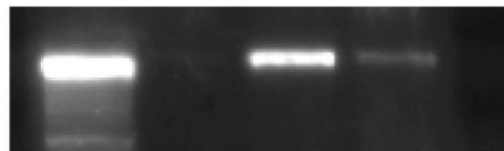
Image collected and cropped by CiteAb under a CC-BY license from the following publication: Initial characterization of a Syap1 knock-out mouse and distribution of Syap1 in mouse brain and cultured motoneurons. *Histochem Cell Biol* (2016)

PNS  
Mitochondria  
Cytoplasm  
MAM

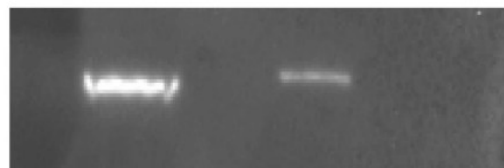
ACSL4



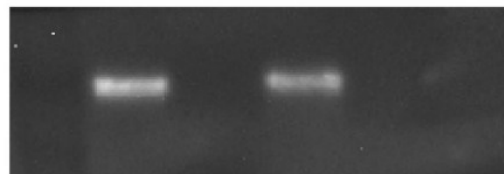
Calnexin



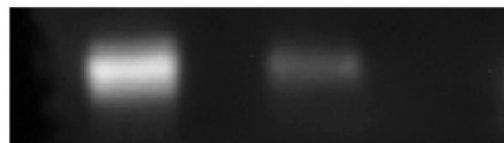
HMGCR



Sigma1R



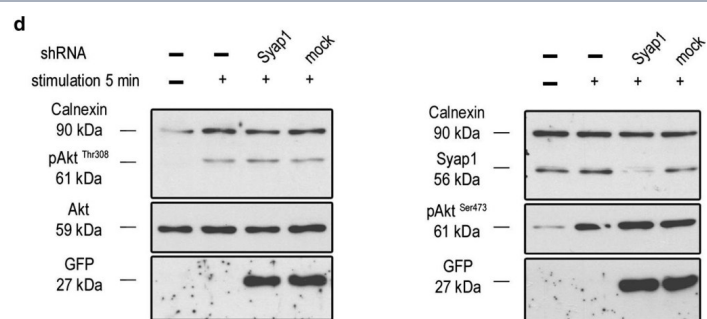
Caveolin



ACSL4 partially localises to MAM. MAM, cytoplasmic and mitochondrial fractions, were prepared from MCF-7 cells. Equal volumes of samples from each MCF-7 fraction were subjected to SDS-PAGE separation and immunoblotted for ACSL4, calnexin, caveolin, HMGCR and Sigma1R. Each panel represents the results of an experiment repeated twice with similar results

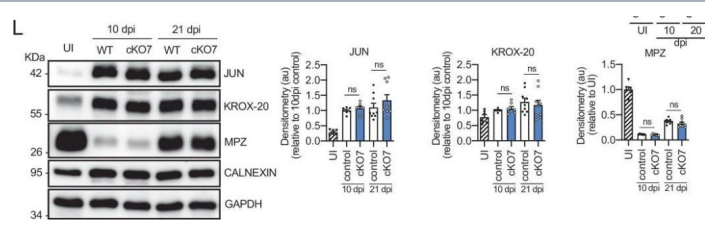
Image collected and cropped by CiteAb under a CC-BY license from the following publication: The endogenous subcellular localisations of the long chain fatty acid-activating enzymes ACSL3 and ACSL4 in sarcoma and breast cancer cells. *Mol Cell Biochem* (2018)





Syap1 knockdown or knockout does not significantly influence total Akt phosphorylation at Thr308 and Ser473 in primary motoneurons. a Western blot of serum-starved cells stimulated with BDNF (20 ng/ml) in a time series ranging from 2 s to 30 min. Maximum Akt Thr308 (left blot) and Ser473 (right blot) phosphorylation is achieved after 2–5 min of neurotrophin stimulation. b Western blots of motoneurons from wild-type and Syap1 knock-out embryos stimulated for 5 min with BDNF did not reveal a reduction in Akt phosphorylation at Thr308 (left blot) or Ser473 (right blot) due to Syap1 knockout. Calnexin and pan-Akt served as loading controls while GFP levels indicate a positive infection of the cells. c, d Blots of Syap1 shRNA-infected motoneurons and uninfected and mock-infected controls stimulated for two (c) or five (d) minutes with BDNF. No differences in Akt phosphorylation at Thr308 (left blots) and Ser473 (right blots) were observed after Syap1 knockdown compared to controls. The detection of Syap1 (right blots) demonstrates the strong reduction in Syap1 protein levels by the knockdown. Quantification of the signals of these and similar blots is shown in Fig. S8

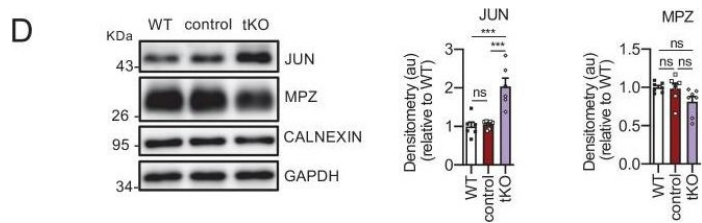
Image collected and cropped by CiteAb under a CC-BY license from the following publication: Initial characterization of a Syap1 knock-out mouse and distribution of Syap1 in mouse brain and cultured motoneurons. *Histochem Cell Biol* (2016)



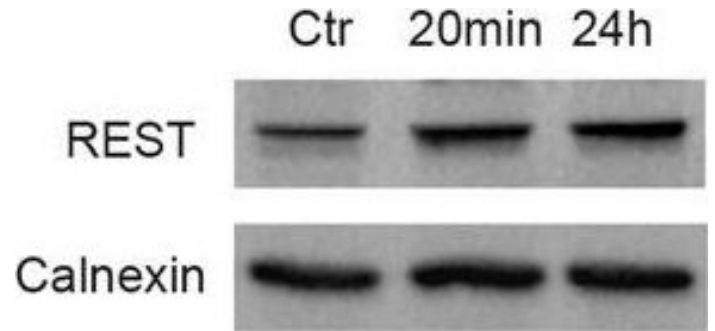
Remyelination in the cKO7 mice. (A) Representative transmission TEM images of P60 sciatic nerves uninjured (UI) and 10 and 20 days post crush (dpi) of cKO7 (Mpz-Cre<sup>+/−</sup>;Hdac7 flx/flx) and the WT control littermates (Mpz-Cre<sup>−/−</sup>;Hdac7 flx/flx) are shown. Scale bar: 5  $\mu$ m. No changes were found at any point in the nerve area (B), the number of myelinated axons (C), g ratios (D), number of unmyelinated axons >1.5  $\mu$ m (E), the total number of unmyelinated axons >1.5  $\mu$ m in a 1:1 relationship with Schwann cells (F), the total axon number (>1.5  $\mu$ m) (G), the total number of sorted axons (H), the total number of Schwann cells (counted as nuclei) (I), the number of myelinating Schwann cells (J) neither the percentage of myelinated axons (K). For these experiments, three to five animals per genotype were used. Unpaired t-test was applied for statistical analysis. (L) A representative Western blot of protein extracts obtained from sciatic nerves UI, 10 and 21 days post crush (pdi) is shown. Densitometric quantification shows no differences between phenotypes. Six to nine mice were used for quantification. To decrease the variability of standardizing for a condition with low expression, normalization was done for conditions with higher protein expression. (M) No changes were found in the mRNA for Jun and Gdnf at 10 dpi. (N) No changes were found for Krox-20, Prx, and Mpz at 10 dpi. RT-qPCR with mouse-specific primers for the indicated genes was performed and normalized to 18S rRNA. Graph shows the percentage of mRNA for each gene in the crush injured (10 dpi) nerve normalized to the uninjured controls. A scatter plot is shown with the results obtained, which include also the mean  $\pm$  standard error (SE). Four mice per genotype were used. Data were analyzed with the unpaired t-test. (O) A representative toluidine blue staining image of 4 days-cut sciatic nerve of cKO7 and control mice is shown. The quantification of intact myelin sheaths shows no changes in the cKO7. Scale bar: 10  $\mu$ m. Three to five animals were used for the experiment. Data were analyzed with the unpaired t-test. Primer sequences and antibodies are listed online (Key Resources Table) (\*p < 0.05, \*\*p < 0.01, \*\*\*p < 0.001; ns: not significant). See source data file one online (graphs source data) for more details.

Image collected and cropped by CiteAb under a CC-BY license from the following publication: A genetic



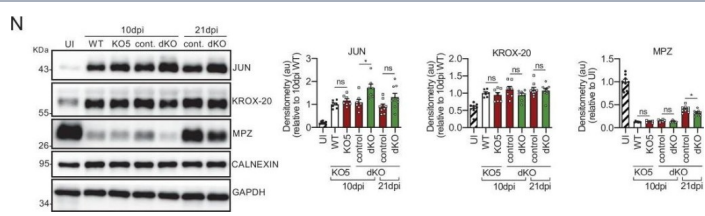


Characterization of the tKO. (A) Representative transmission TEM image of the sciatic nerve of and adult (P60) tKO mouse and a control littermate. Scale bar: 5  $\mu$ m. (B) Scatter plot of g ratio versus axon diameter. 1100 axons of 4 different mice per genotype were used. No changes in g ratio were detected. (C) mRNA for Jun remains increased in the tKO by 2.6-fold ( $1.88 \pm 0.19 \times 10^{-4}$  au in the tKO versus  $0.72 \pm 0.05 \times 10^{-4}$  au in controls;  $p = 0.003$ ) whereas Mpz was slightly decreased ( $1.57 \pm 0.13 \times 10^{-2}$  au in the tKO versus  $2.13 \pm 0.05 \times 10^{-2}$  au in controls;  $p = 0.027$ ). RT-qPCR with mouse-specific primers for the indicated genes was performed. Graph shows a scatter plot for the  $\Delta$ Ct (which include also the mean  $\pm$  standard error [SE]) of the gene normalized to the housekeeping 18S. Five mice per genotype and age were used. Data were analyzed with the unpaired t-test. (D) JUN and MPZ protein levels. A representative Western blot of protein extracts from wild-type (C57BL/6), control and tKO sciatic nerves is shown. The densitometric analysis of six to seven different experiments normalized to WT is also shown. Data were analyzed with the unpaired t-test. Only for JUN was detected consistent changes ( $2.04 \pm 0.22$  in the tKO versus  $1.05 \pm 0.04$  in controls;  $p = 0.0003$ ) at the protein level ( $***p < 0.001$ ). (E) Failed segregation of the axons in the Remak bundles of the tKO. A representative high power TEM image is shown. Morphometric analysis shows that axon diameter distribution is preserved in the tKO, but the number of axons per Remak bundle and the distribution of axon per pocket is changed. Five hundred axons from four animals per genotype were counted. Mixed model analysis of variance (ANOVA) with Bonferroni post hoc test was used for comparisons. Scale bar: 1  $\mu$ m. (F) Pie chart and DEG heatmap of the RNA-seq analysis of P60 showing the distribution of changed genes in the tKO. (G) Volcano plot shows that the most robustly changed genes were upregulated. ENSEMBL identification numbers for the 10 most robustly changed genes are shown. (H) List of the 35 most upregulated genes in the adult (P60) KO classified by FDR. (I) List of the 35 most downregulated genes in the adult (P60) tKO classified by FDR ( $*p < 0.05$ ;  $**p < 0.01$ ;  $***p < 0.001$ ; ns: no significant). See source data file one online (graphs source data) for more details. Characterizing the tKO mice. (A) Representative

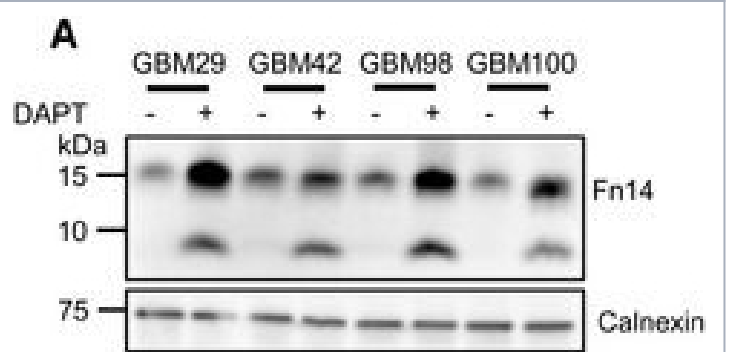


Expression of REST is selectively regulated by IL-1 $\beta$  in primary cortical neurons. a qRT-PCR analysis of REST mRNA levels upon treatment with the indicated pro-inflammatory cytokines for 24 h. b Representative immunoblot (left) and corresponding quantification (right) of REST protein levels under the same experimental conditions. c qRT-PCR analysis of REST mRNA levels upon IL-1 $\beta$  treatment for various times, as indicated. d Representative immunoblot (left) and corresponding quantification (right) of REST protein levels upon treatment with IL-1 $\beta$  for 20 min and 24 h, as compared to control condition. e, f qRT-PCR analysis (e) and immunoblotting (f) of REST4 upon exposure to either IL-1 $\beta$  or vehicle (Veh) for 24 h. g The mRNA levels of the Na $^{+}$  channel NaV1.2 (Scn2a) and synapsin I (SynI) were quantified by qRT-PCR in IL-1 $\beta$ -treated neurons and compared to control. Gapdh, Actin, and Hprt1 were used as housekeeping genes in qRT-PCR analyses. Calnexin was used as loading control for western blotting analyses. Bar graphs show mean  $\pm$  sem of at least  $n = 2$  independent experiments with superimposed individual points.  $*p < 0.05$ ,  $**p < 0.01$ ; one-way ANOVA/Bonferroni's tests (a–d); unpaired two-tailed Student's t test (e–g).

Image collected and cropped by CiteAb under a CC-BY license from the following publication:  
Neuroinflammation induces synaptic scaling through IL-1 $\beta$ -mediated activation of the transcriptional repressor REST/NRSF. *Cell Death Dis* (2021)

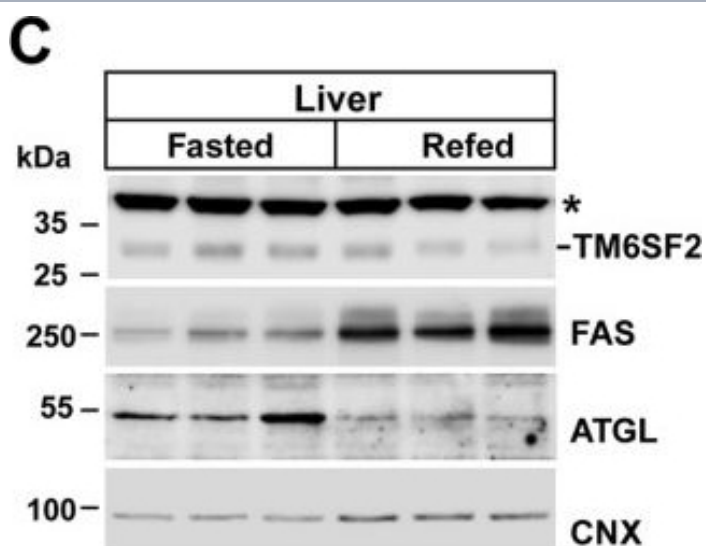


Remyelination is delayed in the nerves of the dKO mice. (A) Representative transmission TEM images of P60 sciatic nerves uninjured (UI) and 10, 20, and 30 days post crush (dpi) of dKO (Mpz-Cre<sup>+/−</sup>; Hdac4flx/flx; Hdac5<sup>−/−</sup>) and the control (Mpz-Cre<sup>−/−</sup>; Hdac4flx/flx; Hdac5<sup>−/−</sup>) littermates are shown. Scale bar: 5  $\mu$ m. (B) No statistically significant differences were observed in the area of the dKO nerves and control littermates (UI:  $p = 0.804$ ; 10 dpi:  $p = 0.195$ ; 20 dpi:  $p = 0.559$ ; 30 dpi:  $p = 0.0594$ ). (C) The number of myelinated axons is notably decreased at 10 dpi ( $388 \pm 55$  in the dKO versus  $1.889 \pm 330$  in the control;  $p = 0.0005$ ). (D) g ratio was increased at 10 dpi ( $0.989 \pm 0.003$  in the dKO versus  $0.934 \pm 0.015$  in control [ $p = 0.002$ ]) and at P21 ( $0.776 \pm 0.003$  in the dKO versus  $0.767 \pm 0.003$  in control [ $p = 0.043$ ]). (E) The number of unmyelinated axons in a 1:1 relationship with Schwann cells was notably increased at 10 dpi ( $2.969 \pm 203$  in the dKO versus  $1.512 \pm 119$  in controls;  $p = 0.0007$ ) and at 20 dpi ( $224 \pm 25$  in the dKO versus  $88 \pm 14$  in controls;  $p = 0.0016$ ). (F) The total number of unmyelinated axons in a 1:1 relationship with Schwann cells is increased at 10 dpi ( $2.148 \pm 155$  in the dKO versus  $1.158 \pm 56$  in the control;  $p = 0.0011$ ) at 20 dpi ( $175 \pm 20$  in the dKO versus  $68 \pm 12$  in the control;  $p = 0.002$ ) and at 30 dpi ( $63 \pm 17$  in the dKO versus  $22 \pm 5$  in the control;  $p = 0.043$ ). (G) No changes in the total axon number was found (UI:  $p = 0.157$ ; 10 dpi:  $p = 0.910$ ; 20 dpi:  $p = 0.349$ ; 30 dpi:  $p = 0.666$ ). (H) Neither in the total sorted axon number (UI:  $p = 0.193$ ; 10 dpi:  $p = 0.169$ ; 20 dpi:  $p = 0.294$ ; 30 dpi:  $p = 0.682$ ). (I) The total number of Schwann cells (counted as nuclei) was increased at 20 dpi ( $861 \pm 34$  in the dKO versus  $630 \pm 53$  in controls;  $p = 0.0041$ ). (J) In contrast, the number of myelinating Schwann cells was found decreased at 10 dpi ( $35 \pm 8$  in the dKO versus  $164 \pm 37$  in controls;  $p = 0.0032$ ). (K) The percentage of myelinated axons is decreased at 10 dpi ( $15.5 \pm 2.3\%$  in the dKO versus  $60.4 \pm 4.8\%$  in controls;  $p < 0.0001$ ), 20 dpi ( $96.6 \pm 0.4\%$  in the dKO versus  $98.8 \pm 0.2\%$  in controls;  $p = 0.0016$ ) and, although much less, at P21 ( $98.9 \pm 0.3\%$  in the dKO versus  $99.6 \pm 0.1\%$  in controls;  $p = 0.0482$ ). For these experiment, three to six animals per genotype were used; unpaired t-test was applied for statistical analysis. (L) Expression of several negative regulators of myelination and repair Schwann cell markers is enhanced at 10 dpi in the sciatic nerves of the dKO: Jun (1.51 fold;  $p = 0.0056$ ), Gdnf (1.85 fold;  $p = 0.0025$ ).

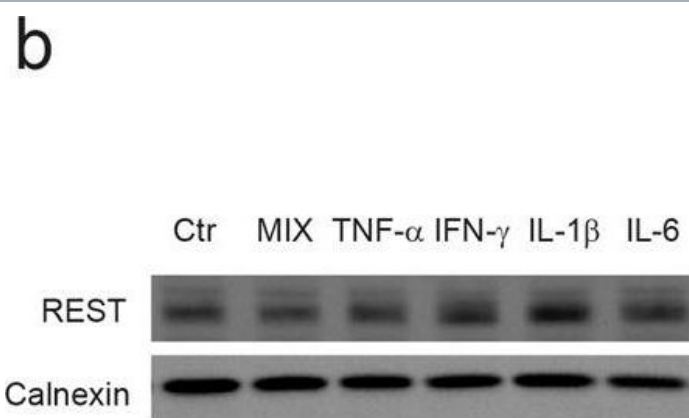


$\gamma$ -Secretase mediates proteolysis of Fn14 in primary cells from human glioblastoma biopsy samples. Cellular Fn14 in ex vivo glioblastoma samples increased upon  $\gamma$ -secretase inhibition. Primary cells from four different glioblastomas were treated with DAPT (1  $\mu$ M) or vehicle overnight. Lysates were blotted against Fn14 and calnexin as loading control. Quantification of the blot in panel (A). For each glioblastoma, the relative (rel.) mean intensity of the normalized Fn14 vehicle condition was used for normalization. sFn14 was strongly reduced upon  $\gamma$ -secretase inhibition in primary GBM cells. Conditioned media of the treated cells from panel (A) were collected after overnight DAPT (1  $\mu$ M) or vehicle treatment. sFn14 levels in these samples were measured by human Fn14 ELISA. Data information: All quantification data are shown as mean  $\pm$  SEM. The tested conditions were compared against their corresponding control (DMSO) condition using two-tailed unpaired t-tests. The P-values that are above 0.05 have not been included into the panels. For all the panels, three biological replicates were performed. Source data are available online for this figure.

Image collected and cropped by CiteAb under a CC-BY license from the following publication: Proteolytically generated soluble Tweak Receptor Fn14 is a blood biomarker for  $\gamma$ -secretase activity. *EMBO Mol Med* (2022)



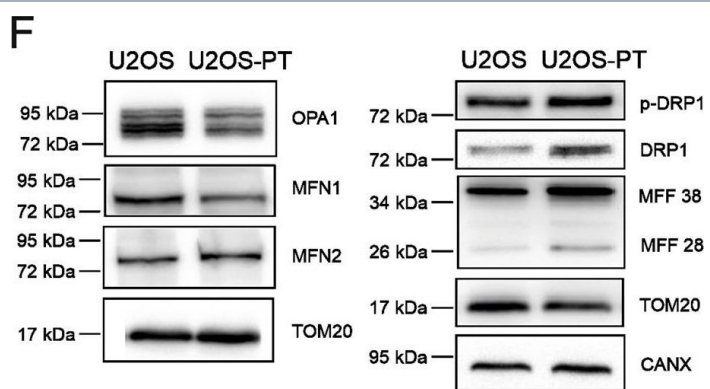
Expression of Tm6sf2 and generation of Tm6sf2<sup>-/-</sup> mice. A, total RNA was extracted from the indicated tissues of WT female mice (n = 3, age = 14 weeks) after a 4-h fast and subjected to quantitative real-time PCR as described under “Experimental Procedures.” The mean ± S.E. (error bars) levels of TM6SF2 transcript in each tissue are expressed relative to the expression level in the ileum, which was arbitrarily set to 1. B, regulation of TM6SF2 expression in response to fasting and refeeding. Mice were entrained to a synchronized feeding regimen for 3 days and then killed after a 24-h fast (Fasted) or after 18 h of fasting and 6 h of refeeding (Refed) (4 male mice, age = 8 weeks). Jejunal and liver proteins (60 µg/well) were size-fractionated by 10% SDS-PAGE, and immunoblotting analysis was performed using antibodies against TM6SF2 and calnexin. C (left), liver proteins (60 µg/well) from the experiment described in B were size-fractionated on an SDS-10% polyacrylamide gel. Fatty acid synthase (FAS) and adipose TG lipase (ATGL) and were used as positive controls for fasting and refeeding, and calnexin (CNX) was used as a loading control in this experiment. C (right), immunoblotting signals were quantified using a LI-COR Odyssey Fc imager. D, Tm6sf2<sup>-/-</sup> mice were generated as described under “Experimental Procedures.” Genotyping was performed by PCR using oligonucleotides (arrows) to amplify a 470-bp (WT) or 400-bp (KO) fragment from genomic DNA. E (left), RNA was isolated from livers of male WT and KO mice (n = 3 male mice/group, 14 weeks old), and TM6SF2 expression was determined by quantitative real-time PCR as described under “Experimental Procedures.” The level of TM6SF2 transcript in WT mice was arbitrarily set to 1. E (right), immunoblotting analysis of hepatic TM6SF2 in 7-week-old female WT and KO mice. Liver lysates and membranes were prepared as described under “Experimental Procedures.” Aliquots of each fraction (50 µg) were size-fractionated by SDS-PAGE, and immunoblotting was performed using a



Expression of REST is selectively regulated by IL-1β in primary cortical neurons. a qRT-PCR analysis of REST mRNA levels upon treatment with the indicated pro-inflammatory cytokines for 24 h. b Representative immunoblot (left) and corresponding quantification (right) of REST protein levels under the same experimental conditions. c qRT-PCR analysis of REST mRNA levels upon IL-1β treatment for various times, as indicated. d Representative immunoblot (left) and corresponding quantification (right) of REST protein levels upon treatment with IL-1β for 20 min and 24 h, as compared to control condition. e, f qRT-PCR analysis (e) and immunoblotting (f) of REST4 upon exposure to either IL-1β or vehicle (Veh) for 24 h. g The mRNA levels of the Na<sup>+</sup> channel NaV1.2 (Scn2a) and synapsin I (SynI) were quantified by qRT-PCR in IL-1β-treated neurons and compared to control. Gapdh, Actin, and Hprt1 were used as housekeeping genes in qRT-PCR analyses. Calnexin was used as loading control for western blotting analyses. Bar graphs show mean ± sem of at least n = 2 independent experiments with superimposed individual points. \*p < 0.05, \*\*p < 0.01; one-way ANOVA/Bonferroni's tests (a–d); unpaired two-tailed Student's t test (e–g).

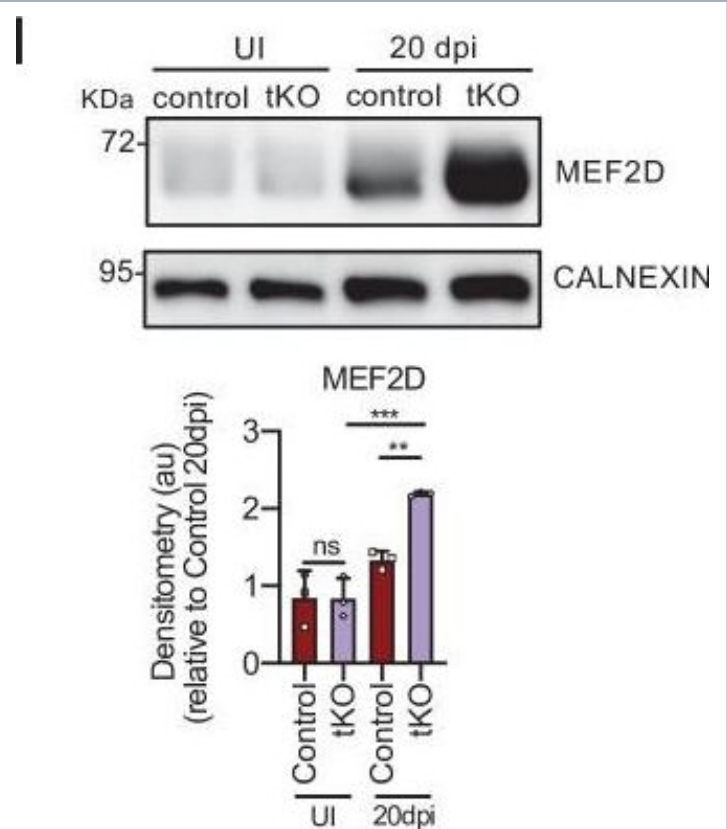
Image collected and cropped by CiteAb under a CC-BY license from the following publication:  
Neuroinflammation induces synaptic scaling through IL-1β-mediated activation of the transcriptional repressor REST/NRSF. *Cell Death Dis* (2021)



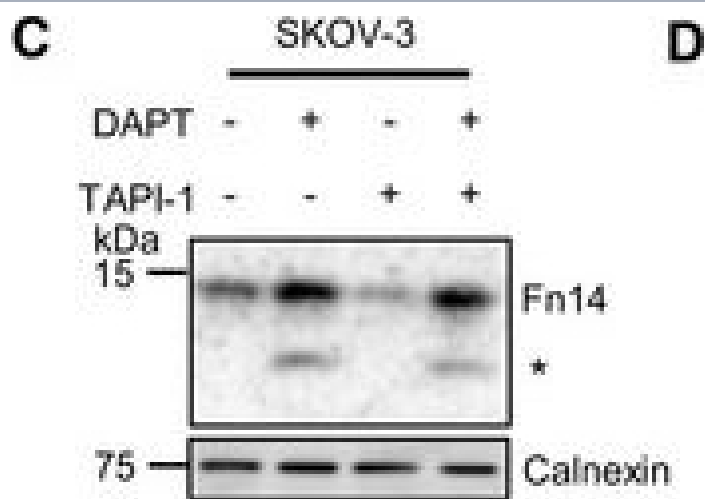


Mitochondria are fragmented in CDDP resistant cells. A Images of mitochondrial network in sensitive (2008, U2OS) and resistant (C13, U2OS-PT) cells acquired by confocal microscopy Zeiss using TOM20 immunostaining, 488. Scale bar 20  $\mu$ m. B Mitochondria segmentation was performed using the ImageJ Squash plugin (Rizk et al., 2014); size and morphology features were measured by using Fiji. Data from 15 different cells per cell line. \* $p < 0.05$ , calculated by a two-tailed unpaired t-test comparing resistant vs sensitive cells. C Images of mitochondrial morphology in sensitive (2008, U2OS) and resistant (C13, U2OS-PT) cells acquired by Tecnai G2 (FEI) transmission electron microscope operating at 100 kV; images were collected by a F114 (TVIPS) CCD camera. The TEM images and experiment are performed by the University of Padova electron microscopy facility. Scale bar 1  $\mu$ m and 500 nm. D The morphometric analysis was performed using ImageJ freehand tool (at least 5 cells per sample, at least 50 images/sample). Data are the mean  $\pm$  SEM of three different experiments; \*\* $p < 0.01$ , \*\*\* $p < 0.001$ , calculated by a two-tailed unpaired t-test comparing resistant vs sensitive cells. E, F Expression of OPA1, MFN1, MFN2, MFFs, p-DRP1 and total DRP1. G The optical density (O.D.) was normalized respectively to TOM20; for total DRP1 to  $\beta$ -ACTIN for 2008-C13 or calnexin for U2OS-U2OS-PT in cancer cells sensitive and resistant. The data are expressed as ratio of resistant cells to sensitive. Data are the mean  $\pm$  SEM of 4–5 different experiments; \* $p < 0.05$ ; \*\* $p < 0.01$ , \*\*\* $p < 0.001$ , calculated by a two-tailed unpaired t-test comparing resistant vs sensitive cells. H mRNA expression of genes OPA1, MFN2, DRP1 and H-FIS1 normalized to  $\beta$ -actin for 2008-C13 or calnexin for U2OS-U2OS-PT. The data are expressed as a ratio of resistant cells to sensitive cells set to 1. Data are the mean  $\pm$  SEM of 4–5 different experiments; \* $p < 0.05$ ; \*\* $p < 0.01$ , calculated by a two-tailed unpaired t-test comparing resistant vs sensitive cells.

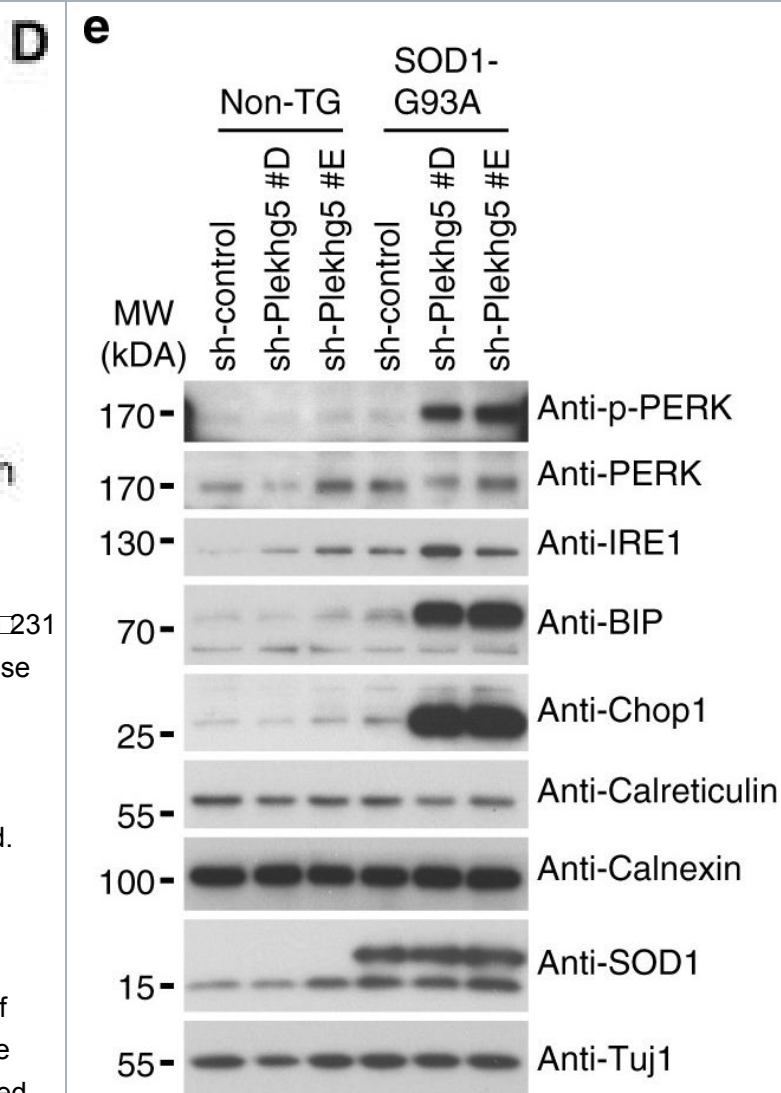
Image collected and cropped by CiteAb under a CC-BY license from the following publication: Cisplatin resistance can be curtailed by blunting Brip3-mediated



MEF2D mediates Hdac9 de novo expression in the tKO. (A) Hdac9 expression is notably induced in the sciatic nerves of the adult (P60) tKO mice ( $6.48 \pm 0.53 \times 10^{-6}$  au the tKO versus  $1.46 \pm 0.28 \times 10^{-6}$  in the control;  $p < 0.0001$ ). Only minor changes were observed in the cKO4 and cKO7. Four to eight mice per genotype were used. Unpaired t-test was used for comparisons. (B) Hdac9 expression is increased from early postnatal development of the tKO nerve. At P2 we found  $1.67 \pm 0.13 \times 10^{-6}$  au in the tKO versus  $0.39 \pm 0.03 \times 10^{-6}$  in the controls ( $p < 0.0001$ ) and at P8 we found  $3.43 \pm 0.52 \times 10^{-6}$  au in the tKO versus  $0.65 \pm 0.09 \times 10^{-6}$  in the controls ( $p < 0.0001$ ). RT-qPCR with mouse-specific primers for Hdac9 was performed. The scatter plot, which include also the mean  $\pm$  standard error (SE), shows the expression of Hdac9 normalized to the housekeeping 18S. Four to five mice per genotype were used. Data were analyzed with the unpaired t-test with Welch's correlation. (C) ChIP-qPCR with anti-H3K9Ac of adult (P60) sciatic nerves of tKO and control mice. Three different experiments of four to five animals per genotype are shown. Data were normalized to the IgG value as shown as relative enrichment. Unpaired t-test was used for comparisons. (D) Alignment of the reads of the RNA-seq from three individual sciatic nerves of control and three tKO mice, both uninjured and at 20 days post crush (20 dpi). Hdac9 gene is transcribed at detectable levels in the sciatic nerve of the uninjured tKO mice, whereas it is almost nondetectable in the control sciatic nerves. The tKO mice (but not the controls) increase additionally the expression of Hdac9 gene during remyelination (20 dpi). (E) mRNA levels of

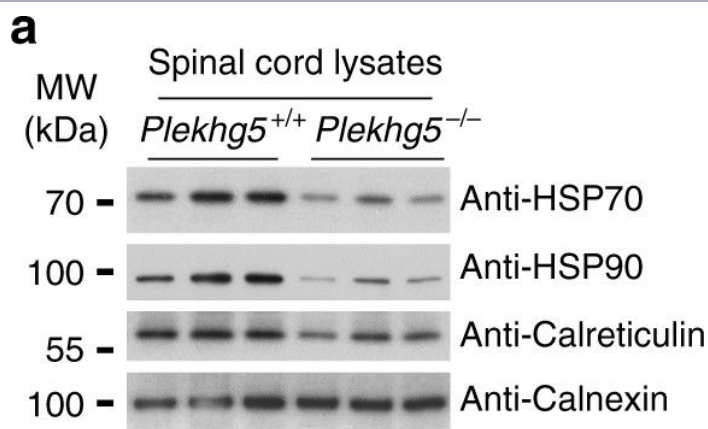


Endogenous Fn14 is processed by protease  $\gamma$ -secretase. Human breast cancer cell line MDA-MB-231 shows cellular accumulation of Fn14 upon  $\gamma$ -secretase inhibition. The cells were treated overnight with  $\gamma$ -secretase inhibitor DAPT (1  $\mu$ M), broad-spectrum metalloprotease inhibitor TAPI-1 (50  $\mu$ M), or the corresponding amount of vehicle DMSO as indicated. Lysates were blotted for Fn14 with an antibody that targets the C-terminal end of the protein, or against calnexin as loading control. The asterisk labels an N-terminally truncated form of Fn14. Quantification of blots from panel (A). The control condition, where the cells were only treated with vehicle (DMSO), was used as baseline, and its average normalized to 1. Human ovarian cancer cell line SKOV-3 shows cellular accumulation of Fn14 upon  $\gamma$ -secretase inhibition. The cells were treated overnight with  $\gamma$ -secretase inhibitor DAPT (1  $\mu$ M), broad-spectrum metalloprotease inhibitor TAPI-1 (50  $\mu$ M), or corresponding amount of vehicle DMSO as indicated. Lysates were blotted for Fn14 with an antibody that targets the C-terminal end of the protein, or against calnexin as loading control. The asterisk labels an N-terminally truncated form of Fn14. Quantification of blot from panel (C). The control condition, where the cells were only treated with vehicle (DMSO), was used as baseline, and its average normalized to 1. sFn14 is reduced upon  $\gamma$ -secretase inhibition in MDA-MB-231 cells. Conditioned media of the treated cells were collected after overnight DAPT (1  $\mu$ M) or vehicle treatment. sFn14 concentration was measured by human Fn14 ELISA. sFn14 is reduced upon  $\gamma$ -secretase inhibition in SKOV-3 cells. Conditioned media of the treated cells were collected after 48 h DAPT (1  $\mu$ M) or vehicle treatment. sFn14 concentration was measured by human Fn14 ELISA. Data Information: All quantification data are shown as mean  $\pm$  SEM. All the panels have N = 3 biological replicates. For panels (B) and (D), the tested conditions were compared against control (DMSO) condition by ordinary one-way ANOVA and Dunnett's multiple comparison test. For



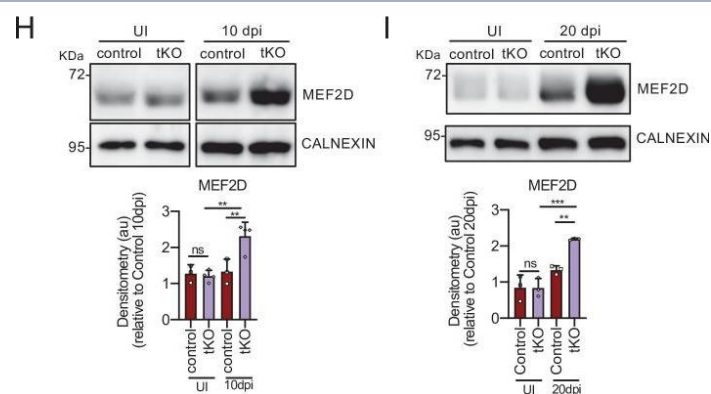
Plekhg5 depletion in SOD1 G93A motoneurons results in elevated ER-stress. a Expression of HSP70, HSP90, Calreticulin, and Calnexin in spinal cord lysates from three animals per genotype. b Quantification of western blot shown in a (each data point represents expression levels of one animal; unpaired t-test; two-tailed). c Expression of IRE1 $\alpha$  and Chop1 in spinal cord lysates from three animals per genotype. d Quantification of western blot shown in c (each data point represents expression levels of one animal; unpaired t-test; two-tailed). e SOD1 G93A and non-transgenic motoneurons were depleted of Plekhg5 and several ER-stress markers were examined after 7 days in culture. f Quantification of western blots shown in e (each data point represents one individual experiment; mean  $\pm$  SEM; unpaired t-test; two-tailed). g Survival of SOD1 G93A motoneurons decreased upon knockdown of Plekhg5 using two independent sh-RNA constructs (each data point represents the % of motoneuron-survival from one individual embryo. At least 50 motoneurons were evaluated from one embryo; mean  $\pm$  SEM; two-way ANOVA; Bonferroni post-test). Images have been cropped for presentation. Full size images are presented in Supplementary Fig. 7



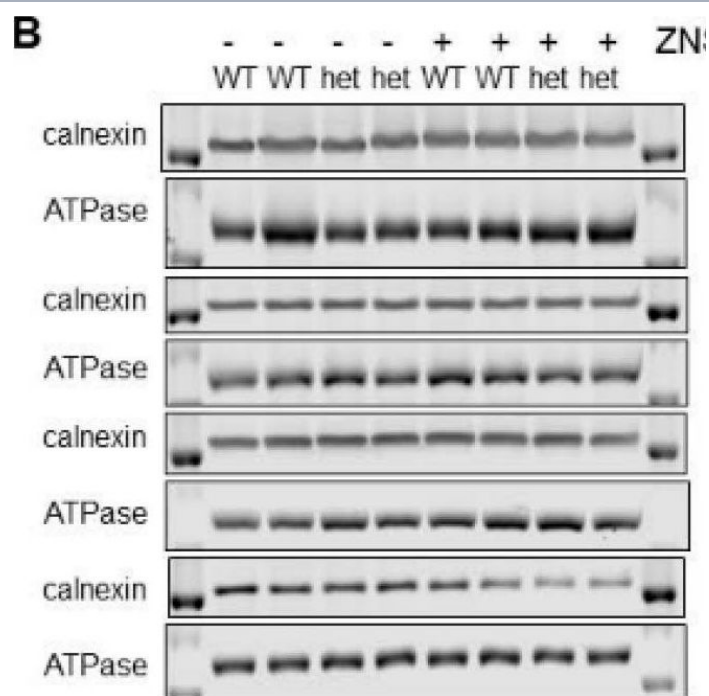


Plekhg5 depletion in SOD1 G93A motoneurons results in elevated ER-stress. **a** Expression of HSP70, HSP90, Calreticulin, and Calnexin in spinal cord lysates from three animals per genotype. **b** Quantification of western blot shown in **a** (each data point represents expression levels of one animal; unpaired t-test; two-tailed). **c** Expression of IRE1 $\alpha$  and Chop1 in spinal cord lysates from three animals per genotype. **d** Quantification of western blot shown in **c** (each data point represents expression levels of one animal; unpaired t-test; two-tailed). **e** SOD1 G93A and non-transgenic motoneurons were depleted of Plekhg5 and several ER-stress markers were examined after 7 days in culture. **f** Quantification of western blots shown in **e** (each data point represents one individual experiment; mean  $\pm$  SEM; unpaired t-test; two-tailed). **g** Survival of SOD1 G93A motoneurons decreased upon knockdown of Plekhg5 using two independent sh-RNA constructs (each data point represents the % of motoneuron-survival from one individual embryo. At least 50 motoneurons were evaluated from one embryo; mean  $\pm$  SEM; two-way ANOVA; Bonferroni post-test). Images have been cropped for presentation. Full size images are presented in Supplementary Fig. 7

Image collected and cropped by CiteAb under a CC-BY license from the following publication: Plekhg5-regulated autophagy of synaptic vesicles reveals a pathogenic mechanism in motoneuron disease. *Nat Commun* (2017)

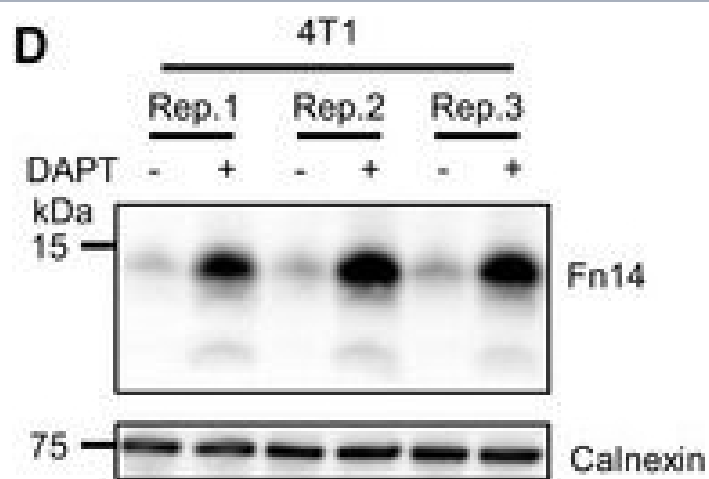


MEF2D mediates Hdac9 de novo expression in the tKO. **(A)** Hdac9 expression is notably induced in the sciatic nerves of the adult (P60) tKO mice ( $6.48 \pm 0.53 \times 10^{-6}$  au the tKO versus  $1.46 \pm 0.28 \times 10^{-6}$  in the control;  $p < 0.0001$ ). Only minor changes were observed in the cKO4 and cKO7. Four to eight mice per genotype were used. Unpaired t-test was used for comparisons. **(B)** Hdac9 expression is increased from early postnatal development of the tKO nerve. At P2 we found  $1.67 \pm 0.13 \times 10^{-6}$  au in the tKO versus  $0.39 \pm 0.03 \times 10^{-6}$  in the controls ( $p < 0.0001$ ) and at P8 we found  $3.43 \pm 0.52 \times 10^{-6}$  au in the tKO versus  $0.65 \pm 0.09 \times 10^{-6}$  in the controls ( $p < 0.0001$ ). RT-qPCR with mouse-specific primers for Hdac9 was performed. The scatter plot, which include also the mean  $\pm$  standard error (SE), shows the expression of Hdac9 normalized to the housekeeping 18S. Four to five mice per genotype were used. Data were analyzed with the unpaired t-test with Welch's correlation. **(C)** ChIP-qPCR with anti-H3K9Ac of adult (P60) sciatic nerves of tKO and control mice. Three different experiments of four to five animals per genotype are shown. Data were normalized to the IgG value as shown as relative enrichment. Unpaired t-test was used for comparisons. **(D)** Alignment of the reads of the RNA-seq from three individual sciatic nerves of control and three tKO mice, both uninjured and at 20 days post crush (20 dpi). Hdac9 gene is transcribed at detectable levels in the sciatic nerve of the uninjured tKO mice, whereas it is almost nondetectable in the control sciatic nerves. The tKO mice (but not the controls) increase additionally the expression of Hdac9 gene during remyelination (20 dpi). **(E)** mRNA levels of Hdac9 (as FPKMs) at 0, 1, 10, and 20 days post crush (dpi) in the RNA-seq experiment. Two-way analysis of variance (ANOVA) was used for statistical comparison. **(F)** Mef2d expression is increased early in development (P8) in tKO nerve ( $1.65 \pm 0.18$  in the tKO versus  $0.97 \pm 0.10$  in controls;  $p = 0.025$ ). RT-qPCR with mouse-specific primers for Mef2d was performed. The scatter plot, which include also the mean  $\pm$  standard error (SE), shows the expression normalized to the housekeeping 18S. Four to five mice per genotype were used. Data

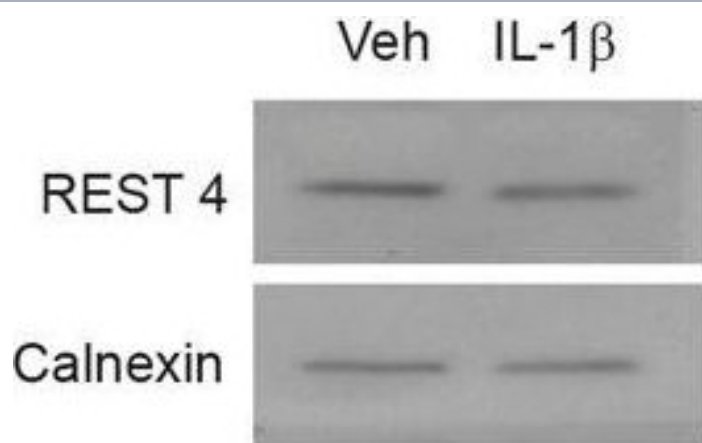


BiP was upregulated in the mutant Gabrg2+/Q390X mice and had a differential response to ZNS compared to the wildtype mice. (A–D) The wildtype and Gabrg2+/Q390X mouse littermates at post-natal day 30–45 were treated with 20 mg/kg ZNS or an equal volume of DMSO/saline vehicle, with daily intraperitoneal injections for 7 days. Brains were dissected, and lysates of the somatosensory cortex (cor), cerebellum (cb), thalamus (thal), and hippocampus (hip) were used for SDS-PAGE. The membranes after SDS\_PAGE were immunoblotted for BiP (1:500) (A,C) or Calnexin (1:500) (B,D). In (C,D), specific protein IDVs were normalized to the loading control, ATPase (1:1000), and then to a paired vehicle-treated wildtype animal. (C,D) N = 6–8 animals. Two-way ANOVA and Šídák’s multiple comparisons. \* p < 0.05 vs. wt ZNS of the same brain region; δ p < 0.05; δδδ p < 0.001 vs. wt vehicle of the same brain region. Values are expressed as the mean ± S.E.M.

Image collected and cropped by CiteAb under a CC-BY license from the following publication: Modulating Endoplasmic Reticulum Chaperones and Mutant Protein Degradation in GABRG2(Q390X) Associated with Genetic Epilepsy with Febrile Seizures Plus and Dravet Syndrome. *Int J Mol Sci* (2024)



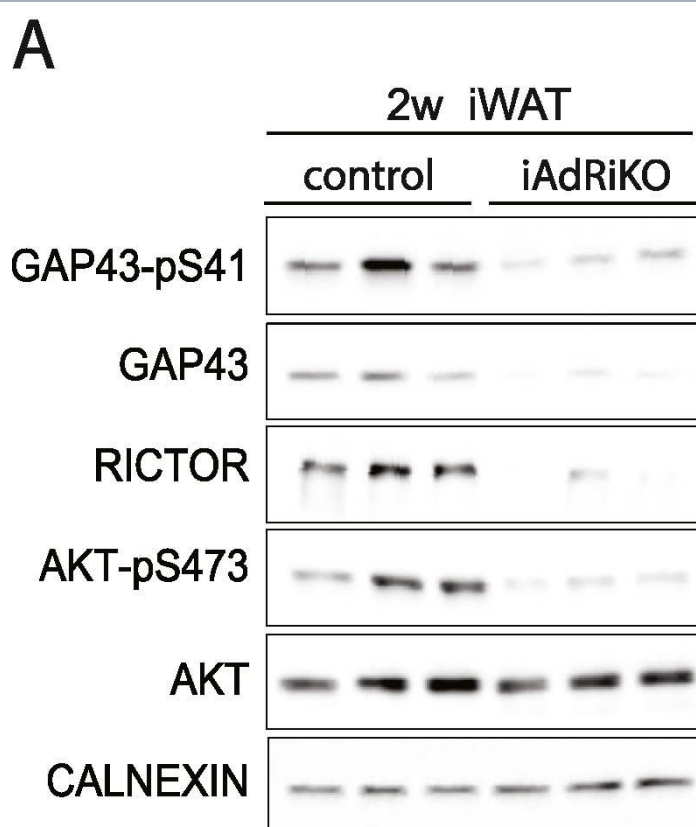
Endogenous Fn14 processing in mouse cell lines by  $\gamma$ -secretase. Mouse glioblastoma cell line GL261 showed cellular accumulation of Fn14 upon  $\gamma$ -secretase inhibition. Cells were treated overnight with  $\gamma$ -secretase inhibitor DAPT (1  $\mu$ M) or vehicle. Lysates of biological replicates (Rep.) were blotted for Fn14 with an antibody that targets the C-terminal end of the protein, or against calnexin as loading control. B Quantification of blot in panel (A). Intensity values of Fn14 were normalized to the respective Calnexin loading control. The average of the control condition, where the cells were only treated with vehicle (DMSO), was consecutively normalized to 1. C Conditioned media of the GL261 cells from panel (A) were collected, and sFn14 levels were measured by ELISA. D Mouse breast cancer cell line 4T1 showed cellular accumulation of Fn14 upon  $\gamma$ -secretase inhibition. Cells were treated overnight with  $\gamma$ -secretase inhibitor DAPT (1  $\mu$ M) or vehicle. Lysates were blotted for Fn14 with an antibody that targets the C-terminal end of the protein, or against calnexin as loading control. E Quantification of blot in panel (D). Intensity values of Fn14 were normalized to the respective calnexin loading control. The average of the control condition, where the cells were only treated with vehicle (DMSO), was consecutively normalized to 1. F Conditioned media of the 4T1 cells from panel (D) were collected and sFn14 levels measured by ELISA. G Mouse ovarian cancer cell line ID8 showed cellular accumulation of Fn14 upon  $\gamma$ -secretase inhibition. Cells were treated overnight with  $\gamma$ -secretase inhibitor DAPT (1  $\mu$ M) or vehicle. Lysates were blotted for Fn14 with an antibody that targets the C-terminal end of the protein, or against calnexin as loading control. H Quantification of blot in panel (G). Intensity values of Fn14 were normalized to the respective calnexin loading control. The average of the control condition, where the cells were only treated with vehicle (DMSO), was consecutively normalized to 1. I Conditioned media of the ID8 cells from panel (G) were collected and sFn14 levels measured by ELISA. J,



Expression of REST is selectively regulated by IL-1 $\beta$  in primary cortical neurons. a qRT-PCR analysis of REST mRNA levels upon treatment with the indicated pro-inflammatory cytokines for 24 h. b Representative immunoblot (left) and corresponding quantification (right) of REST protein levels under the same experimental conditions. c qRT-PCR analysis of REST mRNA levels upon IL-1 $\beta$  treatment for various times, as indicated. d Representative immunoblot (left) and corresponding quantification (right) of REST protein levels upon treatment with IL-1 $\beta$  for 20 min and 24 h, as compared to control condition. e, f qRT-PCR analysis (e) and immunoblotting (f) of REST4 upon exposure to either IL-1 $\beta$  or vehicle (Veh) for 24 h. g The mRNA levels of the Na<sup>+</sup> channel NaV1.2 (Scn2a) and synapsin I (SynI) were quantified by qRT-PCR in IL-1 $\beta$ -treated neurons and compared to control. Gapdh, Actin, and Hprt1 were used as housekeeping genes in qRT-PCR analyses. Calnexin was used as loading control for western blotting analyses. Bar graphs show mean  $\pm$  sem of at least n = 2 independent experiments with superimposed individual points. \*p < 0.05, \*\*p < 0.01; one-way ANOVA/Bonferroni's tests (a–d); unpaired two-tailed Student's t test (e–g).

Image collected and cropped by CiteAb under a CC-BY license from the following publication:

Neuroinflammation induces synaptic scaling through IL-1 $\beta$ -mediated activation of the transcriptional repressor REST/NRSF. *Cell Death Dis* (2021)



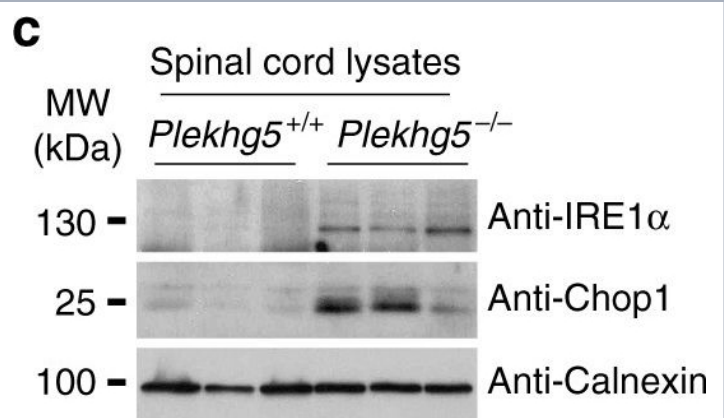
GAP43 expression is downregulated in CGRP-positive neurons upon loss of adipose mTORC2. (A) Immunoblot analysis of inguinal WAT (iWAT) tissue from control and iAdRiKO mice two weeks after tamoxifen treatment. (n = 6; 6). (B) Immunoblot analysis of iWAT tissue from control and iAdRiKO mice four weeks after tamoxifen treatment. (n = 6; 6). (C) Immunoblot analysis of surgically denervated iWAT depot (denervation) compared to iWAT depot from sham-operated mice (sham). Neurofilament heavy polypeptide (NFH). (n = 5; 5). (D) Representative image of a large nerve bundle in iWAT of control mice immunostained with growth-associated protein 43 (GAP43)-pS41 and calcitonin gene-related peptide (CGRP). (N = 11; 9). (E) Representative image of a large nerve bundle in iWAT of control mice immunostained with GAP43-pS41 and tyrosine hydroxylase (TH). (N = 19; 11).

Image collected and cropped by CiteAb under a CC-BY license from the following publication: Adipose mTORC2 is essential for sensory innervation in white adipose tissue and whole-body energy homeostasis. *Mol Metab* (2022)



Syap1 knockdown or knockout does not significantly influence total Akt phosphorylation at Thr308 and Ser473 in primary motoneurons. a Western blot of serum-starved cells stimulated with BDNF (20 ng/ml) in a time series ranging from 2 s to 30 min. Maximum Akt Thr308 (left blot) and Ser473 (right blot) phosphorylation is achieved after 2–5 min of neurotrophin stimulation. b Western blots of motoneurons from wild-type and Syap1 knock-out embryos stimulated for 5 min with BDNF did not reveal a reduction in Akt phosphorylation at Thr308 (left blot) or Ser473 (right blot) due to Syap1 knockout. Calnexin and pan-Akt served as loading controls while GFP levels indicate a positive infection of the cells. c, dBlots of Syap1 shRNA-infected motoneurons and uninfected and mock-infected controls stimulated for two (c) or five (d) minutes with BDNF. No differences in Akt phosphorylation at Thr308 (left blots) and Ser473 (right blots) were observed after Syap1 knockdown compared to controls. The detection of Syap1 (right blots) demonstrates the strong reduction in Syap1 protein levels by the knockdown. Quantification of the signals of these and similar blots is shown in Fig. S8

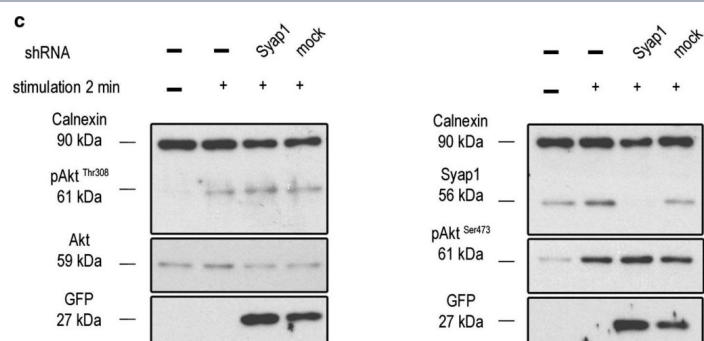
Image collected and cropped by CiteAb under a CC-BY license from the following publication: Initial characterization of a Syap1 knock-out mouse and distribution of Syap1 in mouse brain and cultured motoneurons. *Histochem Cell Biol* (2016)



Plekhg5 depletion in SOD1 G93A motoneurons results in elevated ER-stress. a Expression of HSP70, HSP90, Calreticulin, and Calnexin in spinal cord lysates from three animals per genotype. b Quantification of western blot shown in a (each data point represents expression levels of one animal; unpaired t-test; two-tailed). c Expression of IRE1α and Chop1 in spinal cord lysates from three animals per genotype. d Quantification of western blot shown in c (each data point represents expression levels of one animal; unpaired t-test; two-tailed). e SOD1 G93A and non-transgenic motoneurons were depleted of Plekhg5 and several ER-stress markers were examined after 7 days in culture. f Quantification of western blots shown in e (each data point represents one individual experiment; mean ± SEM; unpaired t-test; two-tailed). g Survival of SOD1 G93A motoneurons decreased upon knockdown of Plekhg5 using two independent sh-RNA constructs (each data point represents the % of motoneuron-survival from one individual embryo. At least 50 motoneurons were evaluated from one embryo; mean ± SEM; two-way ANOVA; Bonferroni post-test). Images have been cropped for presentation. Full size images are presented in Supplementary Fig. 7

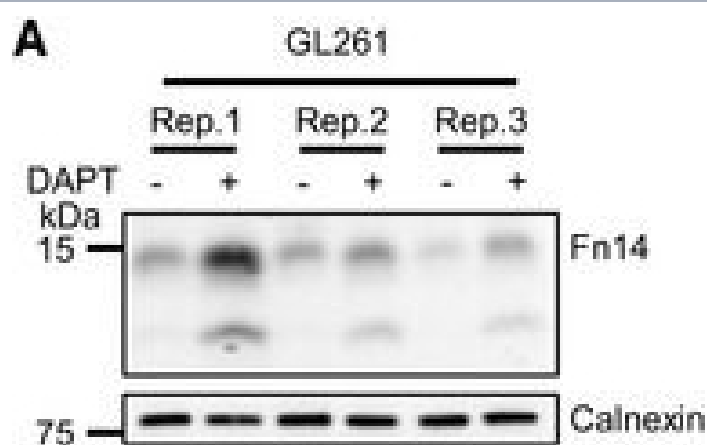
Image collected and cropped by CiteAb under a CC-BY license from the following publication: Plekhg5-regulated autophagy of synaptic vesicles reveals a pathogenic mechanism in motoneuron disease. *Nat Commun* (2017)





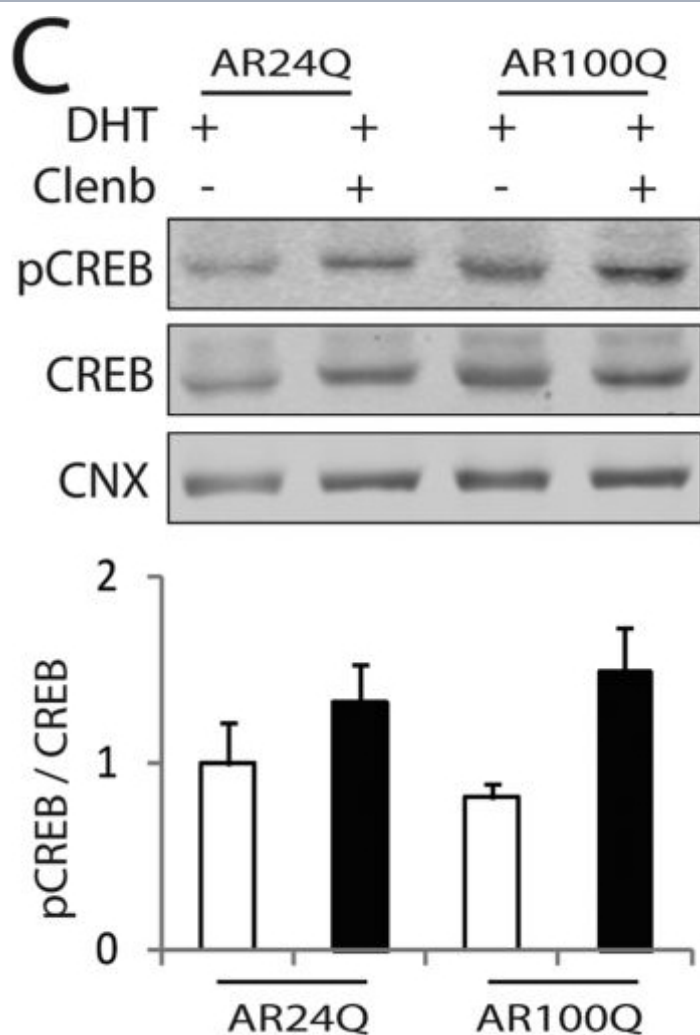
Syap1 knockdown or knockout does not significantly influence total Akt phosphorylation at Thr308 and Ser473 in primary motoneurons. a Western blot of serum-starved cells stimulated with BDNF (20 ng/ml) in a time series ranging from 2 s to 30 min. Maximum Akt Thr308 (left blot) and Ser473 (right blot) phosphorylation is achieved after 2–5 min of neurotrophin stimulation. b Western blots of motoneurons from wild-type and Syap1 knock-out embryos stimulated for 5 min with BDNF did not reveal a reduction in Akt phosphorylation at Thr308 (left blot) or Ser473 (right blot) due to Syap1 knockout. Calnexin and pan-Akt served as loading controls while GFP levels indicate a positive infection of the cells. c, d Blots of Syap1 shRNA-infected motoneurons and uninfected and mock-infected controls stimulated for two (c) or five (d) minutes with BDNF. No differences in Akt phosphorylation at Thr308 (left blots) and Ser473 (right blots) were observed after Syap1 knockdown compared to controls. The detection of Syap1 (right blots) demonstrates the strong reduction in Syap1 protein levels by the knockdown. Quantification of the signals of these and similar blots is shown in Fig. S8

Image collected and cropped by CiteAb under a CC-BY license from the following publication: Initial characterization of a Syap1 knock-out mouse and distribution of Syap1 in mouse brain and cultured motoneurons. *Histochem Cell Biol* (2016)



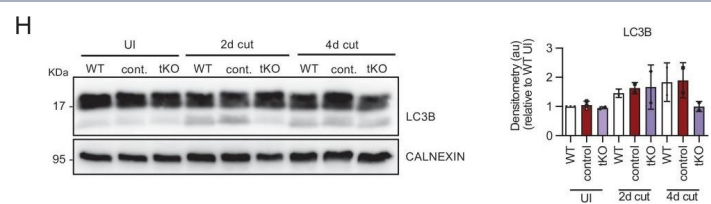
Endogenous Fn14 processing in mouse cell lines by  $\gamma$ -secretase. Mouse glioblastoma cell line GL261 showed cellular accumulation of Fn14 upon  $\gamma$ -secretase inhibition. Cells were treated overnight with  $\gamma$ -secretase inhibitor DAPT (1  $\mu$ M) or vehicle. Lysates of biological replicates (Rep.) were blotted for Fn14 with an antibody that targets the C-terminal end of the protein, or against calnexin as loading control. B Quantification of blot in panel (A). Intensity values of Fn14 were normalized to the respective Calnexin loading control. The average of the control condition, where the cells were only treated with vehicle (DMSO), was consecutively normalized to 1. C Conditioned media of the GL261 cells from panel (A) were collected, and sFn14 levels were measured by ELISA. D Mouse breast cancer cell line 4T1 showed cellular accumulation of Fn14 upon  $\gamma$ -secretase inhibition. Cells were treated overnight with  $\gamma$ -secretase inhibitor DAPT (1  $\mu$ M) or vehicle. Lysates were blotted for Fn14 with an antibody that targets the C-terminal end of the protein, or against calnexin as loading control. E Quantification of blot in panel (D). Intensity values of Fn14 were normalized to the respective calnexin loading control. The average of the control condition, where the cells were only treated with vehicle (DMSO), was consecutively normalized to 1. F Conditioned media of the 4T1 cells from panel (D) were collected and sFn14 levels measured by ELISA. G Mouse ovarian cancer cell line ID8 showed cellular accumulation of Fn14 upon  $\gamma$ -secretase inhibition. Cells were treated overnight with  $\gamma$ -secretase inhibitor DAPT (1  $\mu$ M) or vehicle. Lysates were blotted for Fn14 with an antibody that targets the C-terminal end of the protein, or against calnexin as loading control. H Quantification of blot in panel (G). Intensity values of Fn14 were normalized to the respective calnexin loading control. The average of the control condition, where the cells were only treated with vehicle (DMSO), was consecutively normalized to 1. I Conditioned media of the ID8 cells from panel (G) were collected and sFn14 levels measured by ELISA. J, K Conditioned media of (J) MDA-MB-231 or (K) SKOV-3





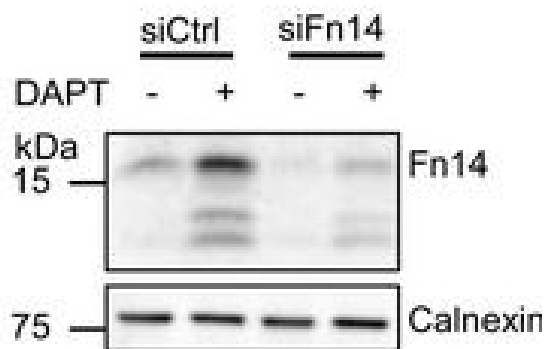
Clenbuterol mitigates the atrophy induced by polyglutamine-expanded AR in C2C12 myotubes. (A) Upper panels, representative bright-field images of C2C12 myotubes expressing AR24Q and AR100Q treated with vehicle, DHT (10 nM), and clenbuterol (clenb, 10  $\mu$ M) for 14 DIV. Bottom panel, myotube width analysis. Graph, mean  $\pm$  SEM,  $n = 3$  independent experiments. Two-way ANOVA + SNK. NS, non-significant. Bar, 25  $\mu$ m. (B,C) Western blotting analysis of phosphorylated and total Akt (B) and CREB (C) in C2C12 myotubes expressing AR24Q and AR100Q and cultured as in (A). Phosphorylated and total Akt and CREB were detected with specific antibodies, and calnexin (CNX) was used as loading control. Graph, mean  $\pm$  SEM,  $n = 6$  (B) and 5 (C) independent experiments. Two-way ANOVA + SNK.

Image collected and cropped by CiteAb under a CC-BY license from the following publication: Beta-agonist stimulation ameliorates the phenotype of spinal and bulbar muscular atrophy mice and patient-derived myotubes. *Sci Rep* (2017)



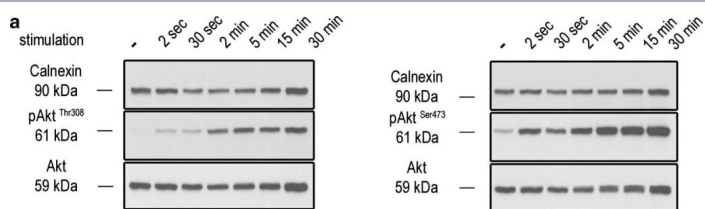
Repair Schwann cell phenotype and myelin removal in the injured tKO.tKO Schwann cells express efficiently markers of the repair phenotype after a cut experiment. In some time points, Jun (A), Olig1 (B), Shh (C), and Ngfr (D) were even more expressed in the tKO than in the control nerves. Mpz was decreased in the UI and at 4 days post cut (E). No changes were found in Gdnf (F). (G) Autophagy gene expression at 4 days after cut was not modified in the tKO nerves. A cut experiment was performed (P60) and sciatic nerves removed at 1, 4, and 7 days postinjury. RT-qPCR with mouse-specific primers for the indicated genes was performed and normalized to 18S rRNA. Graph shows the percentage of mRNA for each gene in the cut injured (4-day cut) nerve normalized to the uninjured controls. A scatter plot is shown with the results obtained, which include also the mean  $\pm$  standard error (SE). Three to five animals per time point and genotype were used, except for uninjured (10–11 nerves). (H) We also found no changes in the activation of LC3B in the tKO nerves by WB during myelin clearance. Data were analyzed with the one-way analysis of variance (ANOVA) Tukey's test. (I) No changes were found in the number of macrophages in the tKO nerves. Representative confocal images of sections obtained from the sciatic nerves of control and tKO mice 4 days after cut are shown. Macrophages were stained with anti F4/80 antibody. Scale bar: 20  $\mu$ m. For the quantification, four animals per genotype were used. Antibodies and primers used are listed in source data section online (Key Resources Table). Data were analyzed with the unpaired t-test (\* $p < 0.05$ , \*\* $p < 0.01$ , \*\*\* $p < 0.001$ ; ns: not significant). See source data file one online (graphs source data) for more details.

Image collected and cropped by CiteAb under a CC-BY license from the following publication: A genetic compensatory mechanism regulated by Jun and Mef2d modulates the expression of distinct class IIa Hdacs to ensure peripheral nerve myelination and repair. *Elife* (2022)

**A**

Surface level of endogenous Fn14 is increased upon  $\gamma$ -secretase inhibition. MDA-MB-231 cells were transfected with an siRNA pool against human Fn14 or nontargeting control (Ctrl) siRNA. A day after transfection, the cells were treated with  $\gamma$ -secretase inhibitor DAPT (1  $\mu$ M) or vehicle overnight. The lysate was collected and blotted against Fn14 (C-terminal antibody) or calnexin as loading control. Shown are representative blots from N = 4 experiments. Quantification of blot in panel (A). The control condition where the cells were only treated with vehicle DMSO and nontargeting siRNA (DMSO + siCtrl) was used as baseline, and its average normalized to 1. N = 4 experiments. MDA-MB-231 cells were transfected and treated as in panel (A). The treated cells were suspended and labeled with ITEM-4 antibody that targets an extracellular site of Fn14, or isotype control. Shown are representative histograms from N = 3 experiments. The mean intensity of the measurement from panel (C). The control condition where the cells were only treated with vehicle DMSO and nontargeting siRNA (DMSO + siCtrl) was used as baseline, and its average normalized to 1. N = 3 experiments. Data information: All quantification data are shown as mean  $\pm$  SEM. The tested conditions were compared against control (DMSO + siCtrl) condition by ordinary one-way ANOVA and Dunnett's multiple comparison test. The P-values that are above 0.05 have not been included into the panels. Number of biological replicates performed is indicated in the corresponding panel legend.

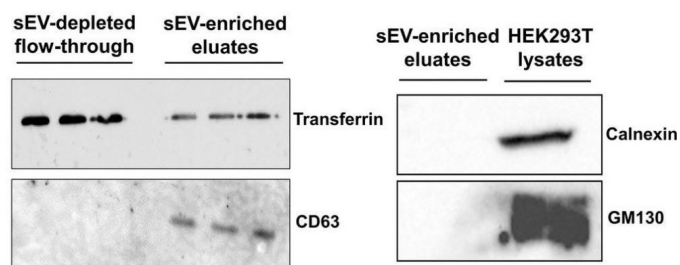
Image collected and cropped by CiteAb under a CC-BY license from the following publication: Proteolytically generated soluble Tweak Receptor Fn14 is a blood biomarker for  $\gamma$ -secretase activity. *EMBO Mol Med* (2022)



Syap1 knockdown or knockout does not significantly influence total Akt phosphorylation at Thr308 and Ser473 in primary motoneurons. a Western blot of serum-starved cells stimulated with BDNF (20 ng/ml) in a time series ranging from 2 s to 30 min. Maximum Akt Thr308 (left blot) and Ser473 (right blot) phosphorylation is achieved after 2–5 min of neurotrophin stimulation. b Western blots of motoneurons from wild-type and Syap1 knock-out embryos stimulated for 5 min with BDNF did not reveal a reduction in Akt phosphorylation at Thr308 (left blot) or Ser473 (right blot) due to Syap1 knockout. Calnexin and pan-Akt served as loading controls while GFP levels indicate a positive infection of the cells. c, d Blots of Syap1 shRNA-infected motoneurons and uninfected and mock-infected controls stimulated for two (c) or five (d) minutes with BDNF. No differences in Akt phosphorylation at Thr308 (left blots) and Ser473 (right blots) were observed after Syap1 knockdown compared to controls. The detection of Syap1 (right blots) demonstrates the strong reduction in Syap1 protein levels by the knockdown. Quantification of the signals of these and similar blots is shown in Fig. S8

Image collected and cropped by CiteAb under a CC-BY license from the following publication: Initial characterization of a Syap1 knock-out mouse and distribution of Syap1 in mouse brain and cultured motoneurons. *Histochem Cell Biol* (2016)

C



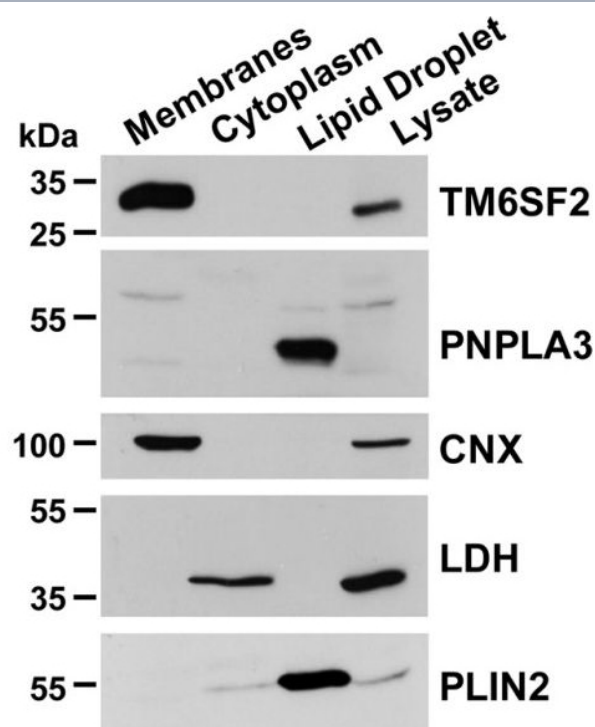
Characterization of serum-derived small extracellular vesicles (sEV). (A) Representative transmission electron microscopy (TEM) images of sEV isolated by exoEasy kit. Scale bars are 500 nm on the left and middle images (magnification  $\times 60,000$ ) and 200 nm on the right image (magnification  $\times 100,000$ ). Spherical membranous particles with an expected size of sEV are indicated with red arrows. (B) Representative particles size distribution profile of nanoparticle tracking analysis (NTA). The calculated size distribution is depicted as a mean (black line) with standard error (red shaded area) along with descriptive summary of particles size. The mean concentration of particles ( $\pm$  standard error) was  $2.73 \times 10^9$  ( $5.71 \times 10^7$ ) particles/ml. Data were analyzed using NanoSight NTA software v3.2

(<https://www.malvernpanalytical.com/en/support/product-support/software/nanosight-nta-software-update-v3-2>).

(C) The expression of CD63 (exosome marker) and transferrin (negative marker) in sEV-enriched eluate and sEV-depleted flow-through was determined by western blotting. The expression of calnexin and GM130 (both negative markers) was also examined in sEV eluate and cell lysate (HEK293T). Full scans of all uncropped images are provided in Supplementary Fig. 1.

Image collected and cropped by CiteAb under a CC-BY license from the following publication: Small RNA sequencing of circulating small extracellular vesicles microRNAs in patients with amyotrophic lateral sclerosis. *Sci Rep* (2023)

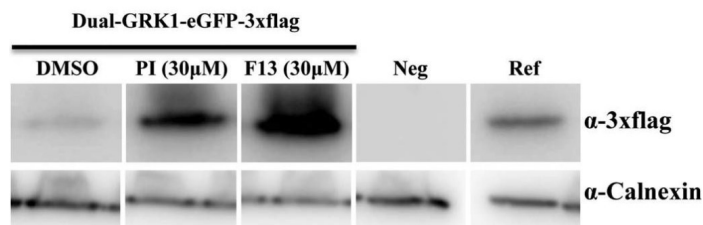
C



Localization of TM6SF2 and neutral lipids in mouse primary hepatocytes. A and B, primary hepatocytes from 8-week-old female WT mice that were fed chow ad lib were plated on coverslips for 4 h, fixed, and stained with BODIPY and with an antibody against TM6SF2 (A) and the LD marker PLIN2 (perilipin 2) (B). All images were taken using a  $\times 63$  oil immersion objective. Scale bar, 10  $\mu$ m. C, female C57Bl/N mice (14 weeks old) were fed a high sucrose diet for 2 weeks. Feeding was synchronized for 3 days, and then the mice were killed at the end of the feeding cycle. Livers were homogenized, and the LDs, membranes, and cytosol were separated by ultracentrifugation as described under "Experimental Procedures." Aliquots of proteins from the membrane and cytosolic fractions (50  $\mu$ g each) and one-tenth of the LD protein was subjected to 10% SDS-PAGE and immunoblotting as described under "Experimental Procedures." Calnexin (CNX), lactate dehydrogenase (LDH), and PLIN2 were used as controls for the ER, cytosolic, and LD fractions, respectively. The experiments were repeated, and the results were similar.

Image collected and cropped by CiteAb under a CC-BY license from the following publication: Inactivation of Tm6sf2, a Gene Defective in Fatty Liver Disease, Impairs Lipidation but Not Secretion of Very Low Density Lipoproteins. *J Biol Chem* (2016)

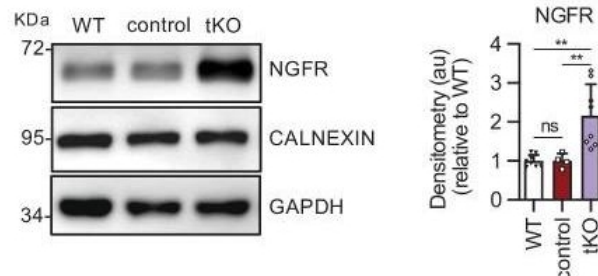
**A**



F13 enhances dual AAV8-mediated transduction of the mouse retina. Representative WB image (A) and quantification (B) of retinal lysates of C57BL/6 eyes co-injected sub-retinally with kinase inhibitors at the indicated concentrations, and dual AAV8 expressing eGFP-3xflag under the control of the PR-specific GRK1 promoter (Dual-GRK1-eGFP-3xflag) or not injected (Neg). For each sample, 65 μg of protein was loaded. Ref, lysate from HEK293 cells transfected with a plasmid expressing eGFP-3xflag used as a reference; α-3xflag, WB with anti-3xflag antibody; α-Calnexin, WB with anti-Calnexin antibody used as loading control; In (B), the values (n = 7), normalized to a standard sample present in every WB, are presented as the mean ± SE. \*p < 0.05.

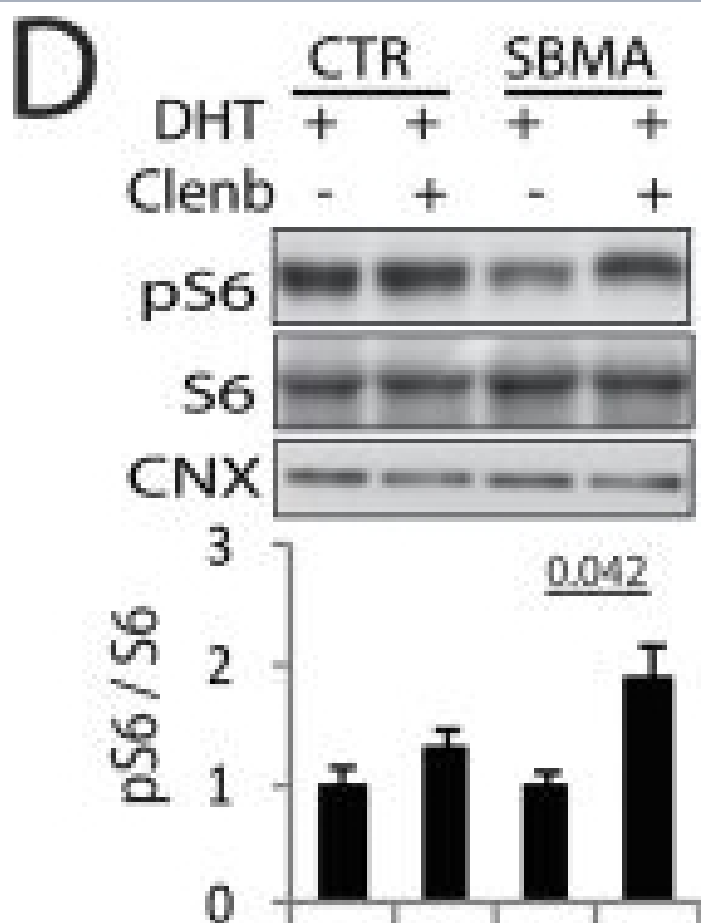
Image collected and cropped by CiteAb under a CC-BY license from the following publication: High-Throughput Screening Identifies Kinase Inhibitors That Increase Dual Adeno-Associated Viral Vector Transduction In Vitro and in Mouse Retina. *Hum Gene Ther* (2018)

**F**

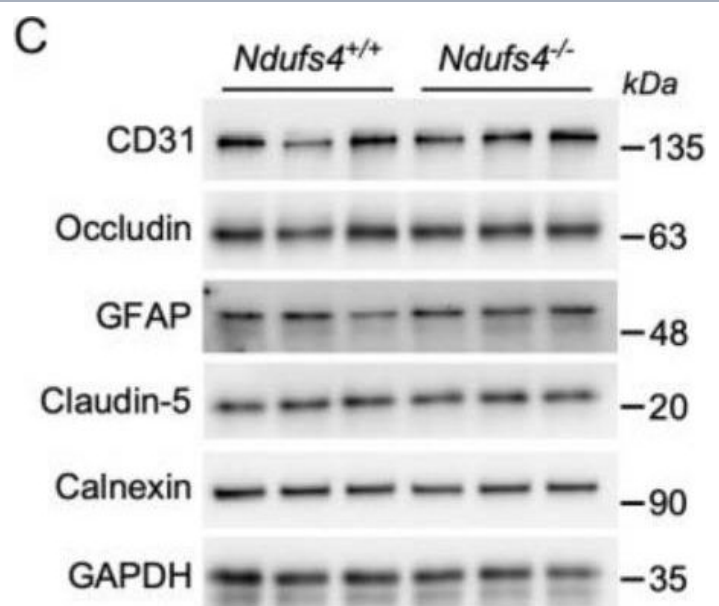


Melanocyte lineage markers are expressed by nonmyelinating Schwann cells of the Remak bundles in the sciatic nerves of the tKO. (A) mRNA for *Tyrp1* is dramatically increased by 1.081-fold in the tKO ( $3.35 \pm 0.71 \times 10^{-4}$  au in the tKO versus  $0.11 \pm 0.05 \times 10^{-6}$  au in controls;  $p = 0.0092$ ) whereas no changes were found in the cKO4, cKO7 neither dKO sciatic nerves. (B) mRNA for *Mcam* is also upregulated (5.13-fold) in the tKO ( $7.39 \pm 0.79 \times 10^{-4}$  au in the tKO versus  $1.44 \pm 0.06 \times 10^{-4}$  au in controls) with only minor or no changes at all for the other genotypes. The same although less marked (1.74-fold) for *Mitf* ( $0.87 \pm 0.09 \times 10^{-5}$  au in the tKO versus  $0.50 \pm 0.02 \times 10^{-5}$  au in controls;  $p = 0.0128$ ) (C) and *Ednrβ* ( $4.1$ -fold;  $4.23 \pm 0.52 \times 10^{-5}$  au in the tKO versus  $1.04 \pm 0.09 \times 10^{-5}$  au in controls;  $p = 0.0032$ ) (D). RT-qPCR with mouse-specific primers for the indicated genes was performed. Graph shows a scatter plot for the  $\Delta Ct$  (which include also the mean ± standard error [SE]) of the gene normalized to the housekeeping 18S. Four to five mice per genotype were used. Data were analyzed with the unpaired t-test with Welch's correlation. (E) MCAM protein levels in the sciatic nerves of the tKO. A representative Western blot of protein extracts from wild-type (C57BL/6), control and tKO sciatic nerves is shown. MCAM protein was increased by 7.6-fold in the tKO ( $9.93 \pm 1.75$  au in the tKO versus  $1.30 \pm 0.13$  in controls;  $p = 0.0003$ ). (F) NGFR protein was increased by 2.15-fold ( $2.16 \pm 0.29$  in the tKO versus  $1.005 \pm 0.09$  in controls;  $p = 0.0003$ ). Four to eight WB of the same number of animals per genotype were quantified. Data were analyzed with the one-way analysis of variance (ANOVA) Tukey's test. (G) MCAM signal colocalizes with SOX10. (H) MCAM signal colocalizes with NGFR. (I) MCAM is not expressed by myelin-forming Schwann cells (MPZ+). (J) Same happens with NGFR. (K) MCAM signal colocalizes with L1cam, a marker of the nonmyelin-forming Schwann cells of the Remak bundles. P60 sciatic nerves were fixed and submitted to immunofluorescence with the indicated antibodies. Nuclei were counterstained with Hoechst. Representative confocal images of sections obtained from the sciatic nerves of wild-type (WT), control, and tKO mice are shown. Scale bar: 20 μm (\*p < 0.05; \*\*p < 0.01; \*\*\*p < 0.001).





Clenbuterol attenuates the toxicity of polyglutamine-expanded AR in SBMA patient-derived myotubes. (A) Representative images of myotubes derived from SBMA patients and age-matched normal subjects (CTR) treated with vehicle, DHT (10 nM), and clenbuterol (Clenb, 10  $\mu$ M) for 10 DIV. Bar, 20  $\mu$ m. (B) Analysis of the width of myotubes derived from CTR subjects and SBMA patients treated as in (A). Graph, mean  $\pm$  SEM,  $n = 3$  CTR subjects, 4 SBMA patients. Two-way ANOVA + SNK. (C) Analysis of the number of nuclei/myotube in myotubes derived from CTR subjects and SBMA patients treated as in (A). Graph, mean  $\pm$  SEM,  $n = 3$  CTR subjects, 5 SBMA patients. Two-way ANOVA + SNK. (D,E) Western blotting analysis of phosphorylated and total S6 and total AR levels in myotubes obtained from CTR subjects and SBMA patients treated as in (A). AR, pS6, and S6 were detected with specific antibodies, and calnexin (CNX) and actin were used as loading control. Graph, mean  $\pm$  SEM,  $n = 3$  CTR subjects and SBMA patients. Two-way ANOVA + SNK. (F) Immunofluorescence analysis of AR in myotubes derived from SBMA patients treated as in (A). AR was detected with a specific antibody and nuclei with DAPI. Shown are representative images of myotubes derived from 3 SBMA patients. Bar, 10  $\mu$ m. (G) Analysis of the number of nuclei/myotube in myotubes derived from CTR subjects and SBMA patients treated with DHT (10 nM) and either vehicle or salbutamol (Salb, 1  $\mu$ M) for 10 DIV. Graph, mean  $\pm$  SEM,  $n = 3$  CTR subjects, 3 SBMA patients. Student's t-test.

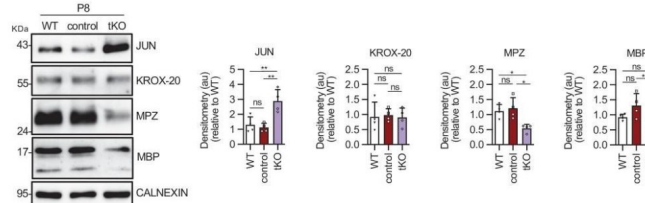


Biochemical and anatomical analysis of cerebral blood vessels. (A) Western blots showing the expression of CD31 and GAPDH in crude brain tissue, the discarded fraction from the purification and the purified fraction containing cerebral blood vessels. (B) Mitochondrial complex I (NADH:ubiquinone oxidoreductase) activity assay from cerebral blood vessels of 1-month-old control ( $n = 3$ ) and *Ndufs4*<sup>-/-</sup> mice ( $n = 5$ ). \*\*\*  $p < 0.001$  (Student's t-test). (C) Western blots showing the expression of CD31, Occludin, GFAP and Claudin-5 in 1-month-old *Ndufs4*<sup>+/+</sup> and *Ndufs4*<sup>-/-</sup>. Calnexin and GAPDH were used as loading controls. (D) Quantification of the Western blots ( $n = 3$  per group, Student's t-test). (E) Images showing a mouse brain before and after the Fast3D clearing protocol. (F) Three-dimensional reconstruction of light sheet fluorescence microscopy images of brains from 1-month-old control and *Ndufs4*<sup>-/-</sup> mice injected with Evans blue. Scale bar: 1.5 mm. (G) Fluorescence scanning microscopy images showing sagittal brain sections from 1-month-old control and *Ndufs4*<sup>-/-</sup> mice stained for CD31 (green) and DAPI (blue). Scale bar: 1.5 mm. Inserts show confocal microscopy images of specific regions marked with squares. Scale bar: 100  $\mu$ m.

Image collected and cropped by CiteAb under a CC-BY license from the following publication: The Blood-Brain Barrier Is Unaffected in the *Ndufs4*<sup>-/-</sup> Mouse Model of Leigh Syndrome. *Int J Mol Sci* (2024)




**N**



Myelin development is notably delayed in the tKO mice. (A) A  $325.1 \pm 48.1\%$  ( $p = 0.0034$ ) increase in the amount of mRNA for *Hdac7* was found in the dKO nerves. No changes in the expression of *HDAC9* were found. RT-qPCR with mouse-specific primers for *Hdac7* was performed and normalized to 18S rRNA. The scatter plot, which include also the mean  $\pm$  standard error (SE), shows the fold change in mRNA normalized to control littermates. Four to eight mice per genotype were used. Data were analyzed with the unpaired t-test. (B) Representative transmission TEM images of P2, P8, and P21 sciatic nerves of tKO mice (Mpz-Cre<sup>+/+</sup>;Hdac4flx/flx;Hdac5<sup>-/-</sup>;Hdac7flx/flx) and the control (Mpz-Cre<sup>-/-</sup>;Hdac4flx/flx;Hdac5<sup>-/-</sup>;Hdac7flx/flx) littermates. Scale bar: 5  $\mu$ m. (C) No statistically significant differences were observed between the area of the tKO nerves and control littermates (P2:  $p = 0.5234$ ; P8:  $p = 0.9279$ ; P21:  $p = 0.9009$ ). (D) The number of myelinated axons is notably decreased at P2 ( $208 \pm 24$  in tKO versus  $1.160 \pm 29$  in controls;  $p \leq 0.0001$ ) and P8 ( $1.487 \pm 179$  in tKO versus  $4.235 \pm 129$  in controls;  $p \leq 0.0001$ ). (E) g ratio was increased at P8 ( $0.80 \pm 0.01$  in the tKO versus  $0.76 \pm 0.01$  in control;  $p = 0.0045$ ). (F) The number of unmyelinated axons in a 1:1 relationship with Schwann cells was notably increased at P8 ( $3.187 \pm 111$  in the tKO versus  $628 \pm 21$  in controls;  $p \leq 0.0001$ ). (G) The total number of sorted axons in a 1:1 relationship with Schwann cells is decreased at P2 ( $1.128 \pm 90$  in the tKO versus  $2.131 \pm 95$  in the control;  $p = 0.0007$ ). (H) The total number of Schwann cells (counted as nuclei) is increased at P8 ( $823 \pm 37$  in the tKO versus  $476 \pm 20$  in controls;  $p \leq 0.0001$ ) and at P21 ( $503 \pm 31$  in the tKO versus  $337 \pm 32$  in controls;  $p \leq 0.0152$ ). (I) In contrast, the number of myelinating Schwann cells is decreased at P2 ( $22 \pm 1$  in the tKO versus  $134 \pm 8$  in controls;  $p \leq 0.0001$ ) and at P8 ( $153 \pm 25$  in the tKO versus  $309 \pm 11$  in controls;  $p = 0.0013$ ). (J) The percentage of myelinated axons is decreased at P2 ( $18.5 \pm 3.7\%$  in the tKO versus  $54.6 \pm 1.1\%$  in controls;  $p \leq 0.0001$ ), P8 ( $31.6 \pm 2.9\%$  in the tKO versus  $54.6 \pm 1.1\%$  in controls;  $p \leq 0.0001$ ) and, although much less, at P21 ( $97.9 \pm 0.4\%$  in the tKO versus  $99.9 \pm 0.0\%$  in controls;  $p = 0.0135$ ). For these experiments, three to four animals per genotype were used; unpaired t-test was applied for statistical analysis. (K) Markers of nonmyelin-forming

**B**



4w iWAT

control iAdRiKO

GAP43-pS41

GAP43

RICTOR

AKT-pS473

AKT

CALNEXIN

GAP43 expression is downregulated in CGRP-positive neurons upon loss of adipose mTORC2. (A) Immunoblot analysis of inguinal WAT (iWAT) tissue from control and iAdRiKO mice two weeks after tamoxifen treatment. ( $n = 6$ ; 6). (B) Immunoblot analysis of iWAT tissue from control and iAdRiKO mice four weeks after tamoxifen treatment. ( $n = 6$ ; 6). (C) Immunoblot analysis of surgically denervated iWAT depot (denervation) compared to iWAT depot from sham-operated mice (sham). Neurofilament heavy polypeptide (NFH). ( $n = 5$ ; 5). (D) Representative image of a large nerve bundle in iWAT of control mice immunostained with growth-associated protein 43 (GAP43)-pS41 and calcitonin gene-related peptide (CGRP). ( $N = 11$ ; 9). (E) Representative image of a large nerve bundle in iWAT of control mice immunostained with GAP43-pS41 and tyrosine hydroxylase (TH). ( $N = 19$ ; 11).

Image collected and cropped by CiteAb under a CC-BY license from the following publication: Adipose mTORC2 is essential for sensory innervation in white adipose tissue and whole-body energy homeostasis. *Mol Metab* (2022)



## Handling & Storage

**Handling** Avoid freeze/thaw cycles.

**Long Term Storage** -20°C

**Shipping** Blue Ice

**Regulatory Status** RUO - Research Use Only

## Product Details

**Alternative Name** CNX

**Application** Electron microscopy, ICC, IF, IHC (PS), IP, WB

**Application Notes** Detects a band of ~90kDa by Western blot.

**Formulation** Liquid. In PBS, pH 7.2, containing 50% glycerol and 0.09% sodium azide.

**GenBank ID** X53616

**Host** Rabbit

**Immunogen** Synthetic peptide corresponding to the sequence near the C-terminus of dog calnexin. The sequence is completely conserved in human, mouse and rat.

**Purity Detail** Protein A affinity purified.

**Recommendation Dilutions/Conditions** Western Blot (1:1,000, colorimetric)Suggested dilutions/conditions may not be available for all applications.Optimal conditions must be determined individually for each application.

**Source** Purified from rabbit serum.

**Species Reactivity** Bovine, Chicken, Dog, Drosophila, Guinea pig, Hamster, Human, Monkey, Mouse, Porcine, Quail, Rabbit, Rat, Sheep, Xenopus

**Technical Info / Product Notes** **Cited samples:**  
[For an overview on cited samples please click here.](#)

UniProt ID

P24643

Worry-free Guarantee

This antibody is covered by our [Worry-Free Guarantee](#)

Last modified: May 29, 2024



ENZO LIFE SCIENCES,  
INC.  
Phone: 800.942.0430  
[info-  
usa@enzolifesciences.com](mailto:info-usa@enzolifesciences.com)

European Sales Office  
ENZO LIFE SCIENCES  
(ELS) AG  
Phone: +41 61 926 8989  
[info-  
eu@enzolifesciences.com](mailto:info-eu@enzolifesciences.com)

Belgium, The Netherlands  
& Luxembourg  
Phone: +32 3 466 0420  
[info-  
be@enzolifesciences.com](mailto:info-be@enzolifesciences.com)

France  
Phone: +33 472 440 655  
[info-  
fr@enzolifesciences.com](mailto:info-fr@enzolifesciences.com)

Germany  
Phone: +49 7621 5500 526  
[info-  
de@enzolifesciences.com](mailto:info-de@enzolifesciences.com)

UK & Ireland  
Phone (UK customers):  
0845 601 1488  
Phone: +44 1392 825900  
[info-  
uk@enzolifesciences.com](mailto:info-uk@enzolifesciences.com)